Hyperspectral Confocal Imaging for High-Throughput Readout and Analysis of Bio-Integrated Laser Particles

Vera M. Titze[1,2,*], Soraya Caixeiro[2], Vinh San Dinh[1], Matthias König[2], Matthias Rübsam[3,4], Nachiket Pathak[2], Anna-Lena Schumacher[5], Maximilian Germer[5], Christian Kukat[5], Carien M. Niessen[3,4], Marcel Schubert[1,2,*], Malte C. Gather[1,2,4,*]

[1] Centre of Biophotonics, School of Physics and Astronomy, University of St Andrews, UK

[2] Humboldt Centre for Nano- and Biophotonics, University of Cologne, Germany

[3] Department Cell Biology of the Skin, University Hospital Cologne, University of Cologne, Germany

[4] Cologne Excellence Cluster on Cellular Stress Responses in Aging-Associated Disease (CECAD), University of Cologne, Germany

[5] FACS & Imaging Core Facility, Max Planck Institute for Biology of Ageing, Cologne, Germany

* correspondence to malte.gather@uni-koeln.de, marcel.schubert@uni-koeln.de, vmt1@st-andrews.ac.uk

Abstract

Integrating laser particles into live cells, tissue cultures, and small animals is an emerging and rapidly evolving technique that offers non-invasive interrogation and labelling with unprecedented information density. The bright and distinct spectra of laser particles make this approach particularly attractive for high-throughput applications requiring single-cell specificity, such as multiplexed cell tracking and intracellular biosensing. To be of practical relevance, the implementation of these applications requires high-resolution, high-speed spectral readout and advanced analysis routines, which leads to unique technical challenges. Here, we present a modular protocol consisting of two separate procedures. The first part of our protocol instructs users on how to efficiently integrate different types of laser particles into living cells. The second part presents a workflow for obtaining intracellular lasing spectra with high spectral resolution and up to 125 kHz readout rate and starts from the construction of a custom hyperspectral confocal microscope. We provide guidance on running hyperspectral imaging routines for various experimental design choices and recommend specific workflows for processing the resulting large data sets along with an open-source Python library of functions covering the entire analysis pipeline. The results one can obtain using this protocol are illustrated with three representative experiments: Rapid, large-volume mapping of absolute refractive index using polystyrene microbead laser particles, intracellular sensing to monitor cardiac contractility with polystyrene microbead laser particles, and long-term cell tracking using semiconductor nanodisk laser particles. Our sample preparation and imaging procedures can be completed within two days. Setting up the hyperspectral confocal microscope for laser particle characterization will take users with little prior experience in optical and software engineering <2 weeks to complete.

Introduction

Micro- and nanolasers are an emerging class of microscopic optical probes with applications in telecommunication, quantum optics, and biomedical sciences. Over the past decade, small versions of these lasers have been integrated directly into various types of living cells[1–3], where their unique optical characteristics provide a large toolbox for novel applications. Hallmarks of laser emission are bright and ultra-narrow emission peaks (spectral linewidth often <100 pm), non-linear emission characteristics, superb signal-to-noise ratios, excellent photostability, and rich information density encoded in their spectra. Consequently, the integration of such lasers can outcompete traditional methods such as fluorescent labels or quantum dots in applications requiring highly multiplexed cell tracking[4,5]. Additionally, the spectra emitted by small lasers are sensitive to changes to their geometry and their local environment[6,7], which has further allowed their use for intracellular sensing[2], including real-time monitoring of cardiomyocyte contractility[8]. Lastly, the bright and narrowband emission of lasers outperforms conventional imaging methods in deep-tissue applications[8,9], and recent advances on NIR and multi-photon excitation[10] further pave the way for applications in large 3D cell culture models and small animals.

1

While initial work on biolasing looked at generating gain and optical feedback within biological structures[11–16], the more common approach today is to introduce largely self-sustained micro- or nanolasers, which are typically sub-micrometer to a few tens of micrometers in size, into biological specimens. It has been shown that various types of cells, including non-phagocytic ones, readily internalize these lasers and that the lasers generally remain internalized without compromising cell viability, even after cellular division[1,3,5,10,17].

Several material platforms and geometries have been explored for biolasing and we will use the term *laser particle* (LP) to collectively describe a micro- or nanoscopic structure that emits coherent light in the visible or near-infrared spectral range—independent of their exact size, shape, or material composition. Common geometries of LPs are whispering-gallery-mode (WGM) resonators including spheres[2,8,18], disks[17,19], and droplets[20,21], spherical Bragg cavities[14,22], or Fabry-Perot resonators like planar cavities[23] and nanowires[4,24–26]. These LPs typically either consist of an inert matrix with high refractive index (> 1.5) that is doped with fluorescent dye to provide optical gain, or of an organic or inorganic semiconductor material. Developing novel lasing mechanisms, cavity geometries or gain materials for LPs is an active area of research[27–31]. In this protocol, we focus on WGM lasers, due to the commercial availability of fluorescent polymer microbeads that readily serve as WGM lasers and due to the growing use of inorganic semiconductor WGM nanodisks lasers in the LP community[5,17,19]. Optical pumping with short laser pulses of sufficient energy stimulates WGM LPs to emit ultra-narrow lasing spectra with characteristic modes. As a basic understanding of the physical parameters affecting these modes and their positions in the laser spectrum is helpful for a more detailed discussion of their applications, a brief introduction is given in Box 1.

Box 1 | Fundamentals of WGM Lasing

WGM lasers consist of convex shaped cavities, in which light is confined to the internal surface by total internal reflection (Figure 1a). Characteristic lasing modes arise at discrete wavelengths $\lambda_{m,p}$ that exhibit constructive interference of the circulating electromagnetic field. The resonance equation

$$m\lambda_{m,p} = \pi\, d n_{\mathrm{eff}} \tag{1}$$

describes the relationship of the peak emission wavelength with the following physical parameters:

m Mode number: All wavelengths satisfying the criterium for constructive interference are characterized by a mode number that is related to the number of interference maxima in the cavity. Depending on properties of the LP, including its size and optical gain material used, one or several of these modes are observed, i.e., single- or multi-mode spectra. (Note that for simplicity we only use the angular momentum mode number m here; the radial and azimuthal mode numbers are typically not required to describe the spectra of LPs[32].)

p Polarization: The circulating electromagnetic field can have 2 orientations with respect to the surface normal of the cavity. Modes that have the electric field parallel or perpendicular to the surface are called transverse-electric (TE, Figure 1b) or transverse-magnetic (TM), respectively. Note that due to confinement effects, e.g., in very thin disk LPs, only one polarization might be observed.

d Diameter: Due to the dependence of the resonant wavelength on the size of the cavity, LPs with different sizes show unique, well-separated mode positions which allows their use as optical barcodes (Figure 1c).

n_{eff} Effective refractive index: The electric field of the cavity modes has an evanescent field component extending typically tens of nanometers away from the resonator surface (Figure 1b); therefore, their modes depend on an effective refractive index term with contributions of both, the internal (n_{int}) and external refractive index (n_{ext}). Consequently, changes in refractive index in the immediate environment of the LPs lead to real-time shifts in the wavelength of the lasing modes (Figure 1d), allowing the use of LP as sensors. Modes of different polarization (TE or TM) are confined inside the LP to different degrees and therefore differ in their effective refractive index, leading to the occurrence of two separate resonance wavelengths for each mode number m.

Applications of the protocol

Cell Tracking
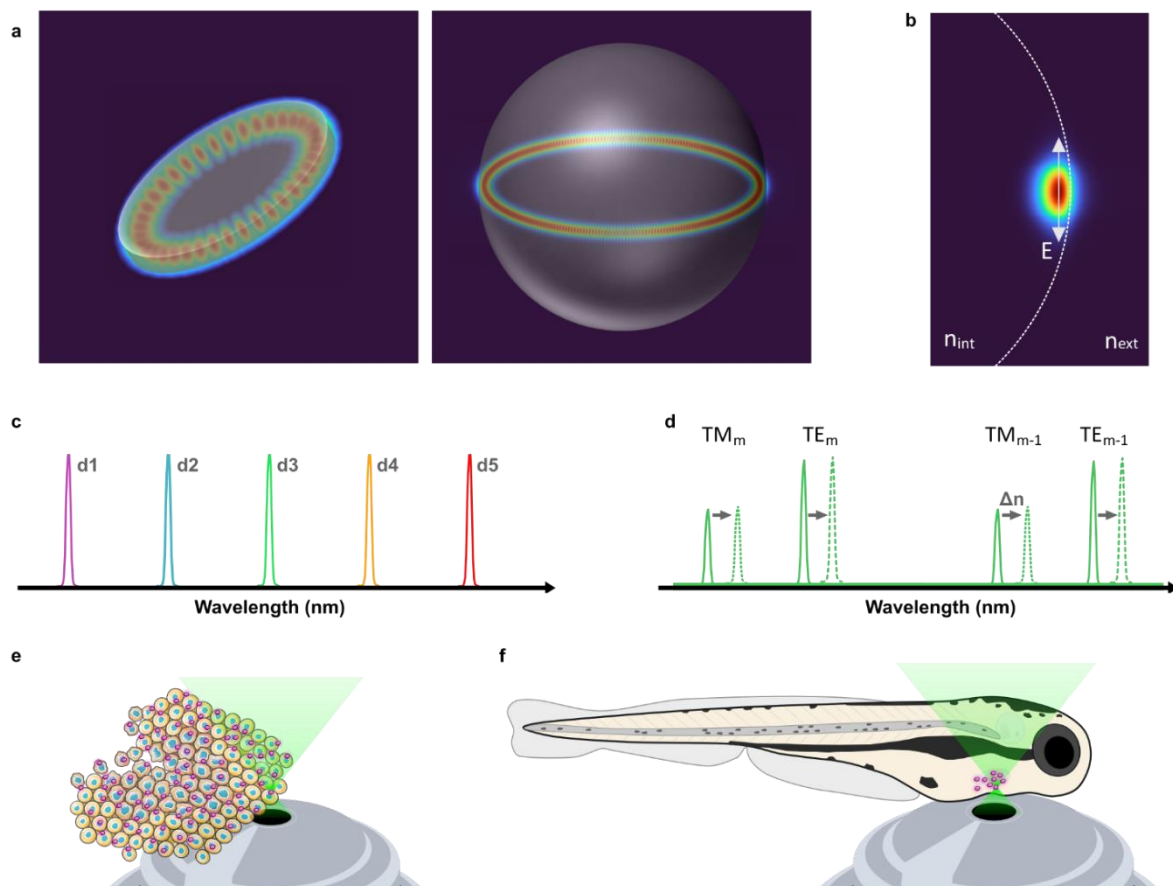
Figure 1 Properties and applications of bio-integrated WGM laser particles. a, 3D rendering of the electric field distribution of WGMs in a nanodisk LP (left, d = 1.7 μm and m = 21) and a microbead LP (right, d = 12 μm and m = 138). **b**, Cross section of the electric field distribution in a microbead LP. The surface of the LP is indicated by the dashed line, and the arrow illustrates the direction of the electric field corresponding to TE polarization. **c**, Illustrative set of single-mode lasing spectra, each resulting from a LP with a different diameter, to create optical barcodes. **d**, Exemplary multi-mode spectrum (solid line) showing two modes (TM/TE) for each angular mode number m. Wavelength shifts of the spectrum (dashed line) can be used for dynamic refractive index sensing. **e**, Schematic showing high-throughput tagging and tracking of cells with intracellular LPs by using their distinct spectra as optical barcodes. **f**, Illustration of deep-tissue applications of LPs for cardiac sensing in live Zebrafish.

Cell tracking applications (Figure 1e) make use of the uniqueness of the spectra emitted by LPs. In smaller single-mode LPs, the position of the mode can be used as a unique tag (Figure 1c)[5,17], and in larger multi-mode resonators, the spacing of adjacent modes (free spectral range), which is related to their size, can be used to re-identify labels[1]. Alternatively, the spectra emitted by multi-mode LPs can be compared to analytical or numerical models to extract their size with very high accuracy (typically better than 1 nm), which then provides a more accurate label for tracking applications[8]. The large number of barcodes that can be generated with LPs is attractive for applications requiring single-cell specificity, particularly where continuous imaging is not possible. Recent applications have included studying the migration of tumor cells[5] and stem cells[4]. Further potential applications include deep-tissue tracking of cells, e.g., in 3D cell culture models or small animals (Figure 1f), where the enhanced penetration depth of multi-photon excitation could complement the resilience of the lasing emission against signal degradation from absorption and scattering in biological tissue[8-10].

Sensing

Intracellular sensing with LPs is achieved by resolving spectral shifts in the laser emission (Figure 1d) that are induced by dynamic changes in the biological environment. These shifts can for example result from

cellular uptake[9,17] or changes in osmotic pressure[2], or they can reflect different stages of the cell cycle[33]. Optical sensing with LPs provides a non-invasive option to follow cellular processes in real time which holds great potential for many applications including disease progression and drug treatment[8,34]. Developing LPs with novel mechanical or chemical properties to achieve more complex sensing mechanisms is an active area of research, and exciting developments include investigating peak splitting to resolve miniscule forces[2], or Foerster Resonance Energy Transfer (FRET)[35–38] to detect changes in the chemical environment. We encourage users to adapt our protocol for the study of such prototype devices, but moving forward, we will focus on commercially available polymer microbead lasers.

Development of the protocol and comparison with other methods

Following our first demonstration of intracellular lasing and cell tracking[1], we published a detailed and quantitative study on the efficiency of LP uptake[3], identifying conditions for reliable integration of polystyrene microbead LPs into different cell types. Specifically, we showed that one can greatly improve the uptake of LPs by the application of a liposome surface treatment. Later, we extended the protocol to the use of semiconductor nanodisk LPs[17], which we fabricate in-house. We also demonstrated integration of polystyrene microbead LPs into living cardiomyocytes to sense cardiac contractility [8]. Other reports of intracellular lasing for cell tracking[4,18,19,39] or intracellular sensing[9] also show successful internalization of LPs by living cells, albeit sometimes described and monitored in less detail.
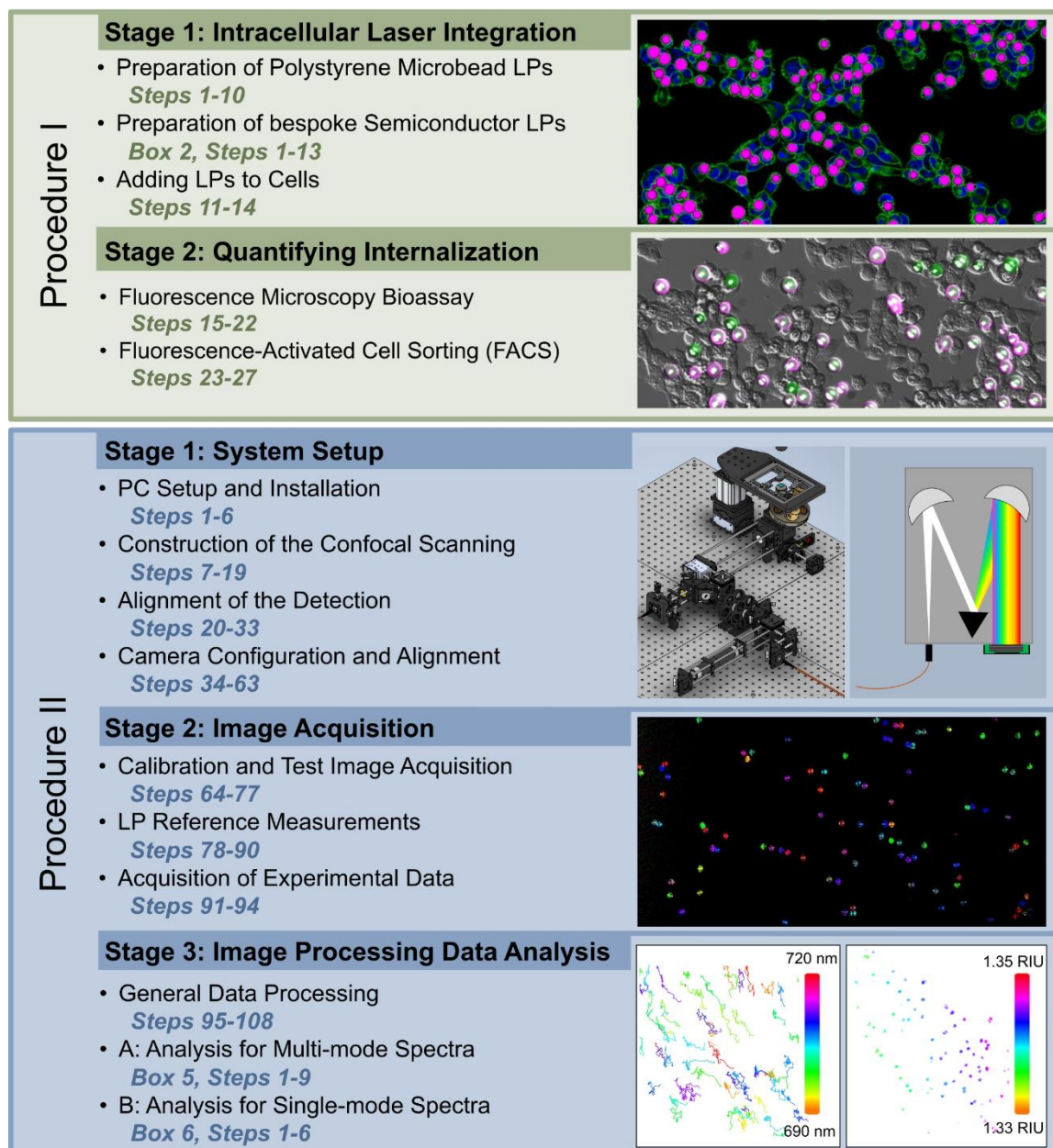
In general, the delivery of cargo with sizes of a few μm into cells is an active area of research, with implications and relevance beyond the use of LPs. It is known that the efficiency of cellular uptake is highly dependent on the geometry and size of the cargo[40,41], as well as on how its surface chemistry interacts with the cell membrane and the cellular uptake machinery[39]. The liposome surface treatments currently used for LP internalization target the latter by facilitating contact with the negatively charged membrane and thus accelerate transfer of LPs through the cell membrane[3]. As an alternative, internalization might be achieved by controlled membrane disruption, but this leads to greater risk of membrane injury and shows poor scalability[42]. Novel biophotonic tools seek to overcome these limitations[43] and might in the future become realistic alternatives for integrating LPs into live cells.

The second crucial step for the successful use of LPs is the recording of the lasing spectra they emit. In a simple characterization setup, the excitation spot produced by the pump laser is scanned over individual LPs, or the sample is moved through the stationary excitation spot, such that the lasing spectra can be collected one-at-a-time on a spectrograph equipped with a CCD camera[1,34]. Our earlier works were conducted on an inverted research microscope, equipped with a pulsed excitation laser to optically pump the LPs, and a high-resolution spectrometer for spectral acquisition. More recently, we additionally implemented automated 3D-scanning of the excitation spot with synchronous high-speed acquisition on a line-scan camera. This combination increases the spectral detection rate by orders of magnitude, enabling high-throughput characterization of LPs, which could be combined with variable excitation schemes including two-photon pumping[10]. The fastest setup based on this approach reported to date collects spectra emitted by LPs at an acquisition rate of up to 10 kHz with synchronous confocal scanning[5,44]. This method was used to track 731 LPs in parallel, but despite the high acquisition rate, recording the spectra for an entire z-stack still took 47 minutes. The most recent version of our setup[10] applies hyperspectral confocal imaging to retrieve the lasing spectra, allowing spectral acquisition rates of up to 125 kHz, as well as scan times as low as 58 s for an extended 3D volume.

Several alternative methods of spectral imaging of LPs have been demonstrated, including a multimodal imaging setup where the spectral readout on the CCD camera is combined with OCT imaging and fluorescence microscopy for rapid identification of the position of LPs, allowing tracking of 13 cells labelled with LPs[4,39]. However, for any application relying on the relatively low frame rate achieved by conventional CCD cameras, scan times quickly become prohibitively long when the numbers of labels increase. A significant improvement in measurement speed was recently achieved by Diffuse Spectral Localization Imaging (DSLI), which applies pushbroom hyperspectral imaging and can retrieve multiple spectra simultaneously in a convoluted form[9]. The DSLI approach was used to image ensembles of LPs with scan times ranging from 10 s to a few minutes, but the required deconvolution of the simultaneously acquired

lasing spectra was only demonstrated for up to 5 individual lasers so far. For applications not requiring spatial information of the sample, a noteworthy alternative to the imaging-based approaches is spectral acquisition in a microfluidic configuration[45]. Integrating a line-scan camera in such a system has enabled spectral acquisition at rates of 25-30 kHz[46].

Overall, among the currently available techniques for the recording of lasing spectra generated by LPs, confocal hyperspectral detection on a line-scan camera offers the highest speed of acquiring individual spectra without sacrificing spectral resolution. Consequently, complex optical setups or deconvolution routines can be avoided, making it the most convenient and most robust approach for high-throughput spectral detection. The confocal detection scheme further provides the most accurate spatial information among the methods discussed above.

Procedure I

Stage 1: Intracellular Laser Integration
- Preparation of Polystyrene Microbead LPs
  Steps 1-10
- Preparation of bespoke Semiconductor LPs
  Box 2, Steps 1-13
- Adding LPs to Cells
  Steps 11-14

Stage 2: Quantifying Internalization
- Fluorescence Microscopy Bioassay
  Steps 15-22
- Fluorescence-Activated Cell Sorting (FACS)
  Steps 23-27

Procedure II

Stage 1: System Setup
- PC Setup and Installation
  Steps 1-6
- Construction of the Confocal Scanning
  Steps 7-19
- Alignment of the Detection
  Steps 20-33
- Camera Configuration and Alignment
  Steps 34-63

Stage 2: Image Acquisition
- Calibration and Test Image Acquisition
  Steps 64-77
- LP Reference Measurements
  Steps 78-90
- Acquisition of Experimental Data
  Steps 91-94

Stage 3: Image Processing Data Analysis
- General Data Processing
  Steps 95-108
- A: Analysis for Multi-mode Spectra
  Box 5, Steps 1-9
- B: Analysis for Single-mode Spectra
  Box 6, Steps 1-6

Figure 2 Schematic of the protocol workflow. The protocol consists of two main procedures. Procedure I describes the experimental recipes required for internalization of LPs by living cells. Following successful uptake, Procedure II focuses on retrieving and analysing the lasing spectra. A custom-built scanning hyperspectral confocal microscope forms the basis of the spectral acquisition. Data generated on such a system can be processed using the open-source analysis toolbox included with the protocol, offering flexible workflows for tracking and sensing applications.

Overview of the procedure

The integration of LPs into living cells is covered as Procedure I in our protocol, along with methods for confirming and quantifying their internalization (Figure 2, top). The acquisition and analysis of the emission generated by LPs is described as Procedure II, which is centered around the construction and operation of a confocal hyperspectral microscope (Figure 2, bottom). A brief overview of variations and design choices of the different parts of the protocol is given below.

Intracellular delivery of LPs

By default, the first Stage of Procedure I is based on commercially available polystyrene microbead LPs. In addition, an alternative set of instructions is provided for the bio-integration of bespoke semiconductor nanolasers since we anticipate our protocol to be also of interest for groups fabricating their own semiconductor LPs. Towards the end of either version of Stage 1, a suspension of LPs in cell culture medium is obtained, which is then incubated with cells to initiate the uptake. In Stage 2, the efficiency of the intracellular delivery can be quantified with methods including a bioassay based on surface staining as well as fluorescence-activated cell sorting (FACS). These sections offer optional, yet highly useful tools for confirming successful cellular integration. (The bioassay based on surface staining requires fixation of the cells and so can only be performed on a control culture that is not required for further experiments or needs to be left until the end of an experiment.) Further alternatives for confirming cellular uptake not covered here are confocal imaging with membrane staining[1], or continuous hyperspectral imaging using LP based refractive index sensing to track cellular uptake events[9,17].

Hyperspectral confocal microscope design

Our hyperspectral confocal microscope consists of two main parts: The confocal scanning optics (Figure 3, Supplementary Figure 1) and the spectroscopy module with high-speed spectral detection. The optical signal is passed through an optical fiber connecting the two parts while an analog trigger signal is used for synchronization of confocal scanning and spectral acquisition. Owing to this modular design, the spectroscopy setup can also be connected to a commercial confocal microscope. The following stages of Procedure II are however focused on the construction of a confocal microscope using free-space optics and assembled from individual, readily available components.
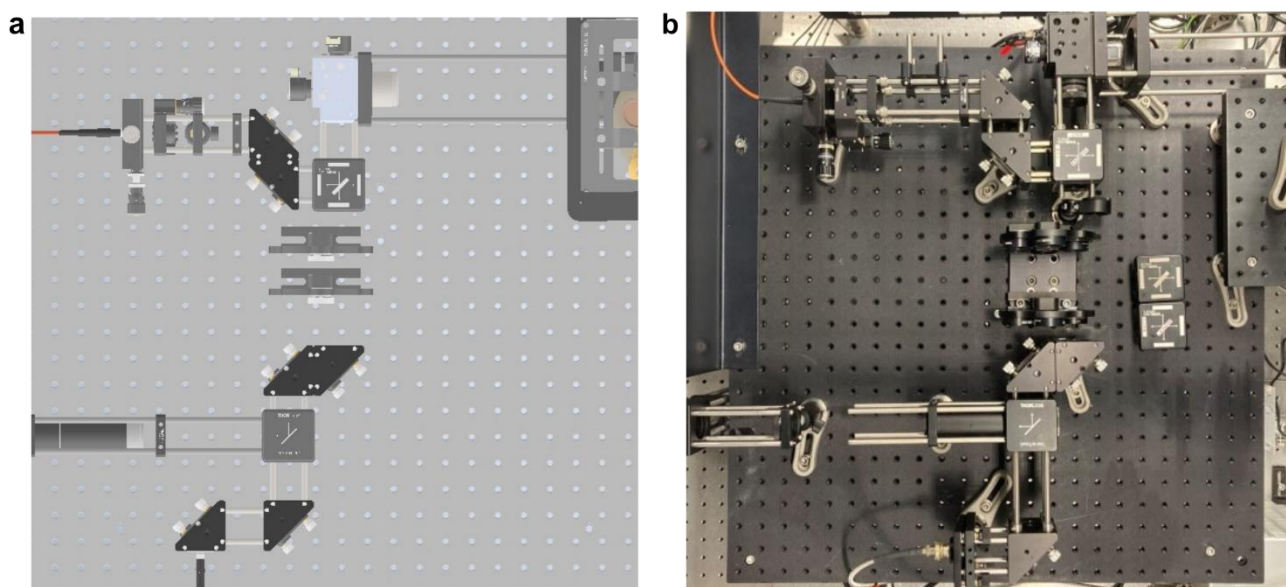
Figure 3 a, CAD rendering and **b**, photograph of the home-built confocal microscope.

To pump the LPs, the excitation laser is raster-scanned across the sample in x-y by a 2D galvo system, while a piezoelectric objective scanner moves the focus along the z-direction. Optical sectioning is achieved by focusing the signal collected from the sample into the optical fiber, which serves as the confocal pinhole of

our system. Using flexible fiber mounts allows to easily switch between fibers with a large core ('open pinhole') and a small core ('closed pinhole'). In some cases, imaging particles with non-linear emission characteristics can greatly enhance the optical sectioning[44,47], where the 'open pinhole' fiber allows flexible and artefact-free coupling of the lasing emission to the spectrometer. We routinely find that the axial resolution is greatly improved by employing the 'closed pinhole' fiber, particularly for large LPs where the closed pinhole rejects emission from lasing paths outside the focal plane.

On the spectrometer side of the fiber, relay optics are used to efficiently couple the signal from the fiber into the spectrograph (Supplementary Figure 2a). The wavelength-dispersed signal can be recorded either by the line-scan camera, or by a low-noise CCD or EMCCD camera connected to the second output of the spectrometer. Having a second camera mounted to the spectrometer is helpful for alignment but not strictly necessary. Lastly, a conventional camera and dia-illumination LED are integrated with the confocal microscope to acquire brightfield images in transmission, which is needed for alignment and for sample navigation.

The scanning of the excitation beam and the movement of the objective scanner are controlled by a data acquisition (DAQ) system and a LabView script. The DAQ also provides the trigger signal that synchronizes the acquisition of a spectrum on the line-scan camera with individual voxels of the confocal scanning. The line-scan camera is operated with custom-built software allowing user-defined acquisition settings for maximum flexibility. This software passes its acquisition settings to the aforementioned LabView script to ensure that the format of the hyperspectral image matches the confocal scan field. We provide step-by-step instructions for installing the setup (Procedure II, Stage 1; Supplementary Table 1 and Supplementary Note 1) and for its operation and calibration (Stage 2).

Data processing workflows

The data processing section (Procedure II, Stage 3) is built on fundamental processing functions required to correctly interpret the highly multidimensional hyperspectral data sets, which can be used for applying calibrations, extracting individual spectra of interest, and visualizing the 3D spatial information showing the positions of all LPs with custom color-coding. We present two additional, more specific workflows for different types of LPs. Workflow A is designed to batch-process spectral information of multi-mode spectra from spherical WGM lasers. Here, the spectral position of the peaks in the recorded spectra are compared to an analytical model of WGMs to determine the size of the microbead and the refractive index in its immediate environment. Further, the variation of refractive index over time can be extracted from the spectra of each individual LP. We include application examples from cardiac contractility[8] sensing and from high-throughput sensing of the diffusion of a glucose solution through an agarose matrix. Workflow B uses hyperspectral images of single-mode LPs to reconstruct their trajectories and extract the evolution of their mode position over time. We demonstrate this capability for a long-term cell tracking experiment, looking at keratinocyte migration in a 3D epidermis model. Results of both workflows can be displayed as x-y-z-t renderings in the Python viewer napari with custom color-coding.

Experimental design

Adaptations

We assume that users of this protocol have varying levels of experience in working with LPs. Therefore, we provide a modular protocol offering flexibility for users who wish to integrate equipment and/or expertise already present in their labs. Our protocol allows substitution of some central components including excitation laser, spectrometer, or parts of the microscope. We particularly encourage users to explore alternative LPs, which are commercially available with different emission ranges spanning the visible spectrum. We also provide information for users who wish to combine our high-speed spectral detection with a commercial confocal microscope, discussing the technical requirements for the microscope and explaining the modifications that need to be made to the optical setup, the camera configuration and the data processing workflows (Supplementary Figures 2b and 3, Supplementary Note 2, Supplementary Table

2). Lastly, the open-source nature of our data processing toolbox will allow users who are comfortable with Python programming to combine and further develop our workflows.

Controls

We typically recommend including two controls: a sample without LPs to look for physiological changes due to the LP integration, and a sample with LPs that is not subjected to the hyperspectral confocal imaging routine to investigate potential effects of phototoxicity. We also recommend checking for successful internalization of the LPs. For sensing of absolute refractive index, we suggest imaging LPs embedded in a medium of homogenous and well-known refractive index as a calibration control measurement.

Expertise and equipment needed to implement the protocol

Prior knowledge of optics, cell culturing, and programming are recommended but not essential for the successful completion of our protocol. Assuming availability of all equipment, the installation, construction, and alignment of the optical system can be completed within 2 weeks. We recommend allocating an area of approximately 2 m^2 on an optical table to house the optics and electronics and using a workstation PC with at least 8 USB ports, two open PCIe x16 slots, and sufficient memory, since the drivers and API of the line-scan camera used in our setup store the camera buffers in the RAM of the workstation PC. The required amount of RAM may vary depending on the desired application, but we would recommend at least 128 GB for any long-term measurements.

Further, we assume that users interested in specific applications of LPs have the appropriate infrastructure and experience, e.g., suitable cell culture facilities and biosafety procedures, as well as access to any materials specific to their application of interest.

Limitations

Intracellular Lasing

In general, the optical quality factor of WGM resonators decreases with decreasing size, which imposes a lower limit on the minimal size that LPs can have[1,48]. To reduce invasiveness and improve uptake efficiency, smaller LPs are preferable. Therefore, we recommend selecting LPs on the smaller side of the range of sufficient optical quality. The quality factor of a WGM resonator also depends on the refractive index contrast between the LP and its environment. As a result, a typical useful size for fluorescent polystyrene beads is 10 – 20 μm, whereas semiconductor nanodisk LPs can reach diameters as small as 0.7 μm.

Further limitations apply to the performance of LPs in the context of tracking and sensing. For tracking applications, a central metric is the number of individual barcodes that can be reliably re-identified. There is some variation depending on the type of LP, but typically, thousands of distinguishable barcodes can be generated[1,46]. This number can be increased significantly via various multiplexing strategies, e.g., by combining multiple LPs within one label[17,49]. However, spectral drift of the LPs, e.g., due to changes in local refractive index can also reduce the number of distinguishable barcodes, a limitation that can be overcome, at least in part, by encapsulation of the LPs.[50] At large excitation pulse energies and average excitation light intensities, the LPs can also show spectral drift due to degradation and accelerated quenching. It is therefore advisable to characterize the spectral stability of the used LPs prior to the final tracking application.

For sensing applications, knowing the limit-of-detection, often defined as the lowest resolvable change in refractive index, is of great importance. We previously reported the limit-of-detection for intracellular sensing with polystyrene microbead LPs to be 5.5×10^{-5} refractive index units (RIU)[8]. Whispering-gallery-mode resonators are among the most sensitive optical sensors[7]. To fully capitalize on this high sensitivity, we recommend prioritizing spectral resolution when procuring instruments and choosing acquisition parameters and applying peak fitting to the measured spectra to further enhance the measurement accuracy.

Finally, for measurements that combine elements of tracking and sensing in a single application, a thorough understanding of the observed modes and their expected behavior is required to decide whether different

spectra originate from different LPs or are generated by the same LP but in different environments. This can be achieved by comparing experimental spectra to a mathematical model, e.g., the one we present for the treatment of multi-mode microbead LPs, as this helps to differentiate between competing effects of size- and refractive index changes.

Hyperspectral Confocal Scanning

Our hyperspectral microscope is designed to run at a spectral acquisition rate of up to 125 kHz. This is equivalent to the maximum speed the line-scan camera can achieve at the preferred bit depth (12 bits). We have refrained from increasing the acquisition rate further for the following reasons: First, even shorter pixel dwell times typically correspond to line rates where non-linearities in the movement of the galvo scanner used here lead to noticeable image distortion. (If needed, this could be addressed by implementing bi-directional scanning or by using a different scan head.) In addition, for acquisition rates above 125 kHz, the camera communication settings must be adjusted, which leads to a reduced bit depth. The resulting reduced dynamic range makes it more challenging to deal with intensity fluctuations, which can occur due to the nonlinearity of the lasing process. It can be necessary to reduce the acquisition speed to below 125 kHz in cases where longer pixel dwell times are required to achieve sufficient signal-to-noise ratios, e.g., when using less efficient LPs or pump lasers with low repetition rates.

The spectral resolution and spectral bandwidth of the system are given by the choice of grating and the focal length of the dispersive spectrometer. The requirements on spectral resolution and bandwidth may vary depending on the type of LP used. The setup described here uses an f=500 mm spectrometer which reaches a spectral resolution of approximately 0.04 nm (at 500 to 700 nm and when employing an 1800 l/mm grating).

The system is designed for visible wavelengths (400 nm – 750 nm). Optical elements in the excitation path are readily replaced by IR-compatible off-the-shelf components (e.g., scan and tube lens, filters, etc.) to allow multi-photon excitation of LPs emitting in the visible range, while IR-emitting LPs will also require different detectors.

Considerations related to balancing imaging speed against signal-to-noise ratio and other factors such as sample size and desired spectral and spatial resolution will be revisited as part of Procedure II of our protocol.

Materials

Reagents

Item	Supplier	Catalog Number	Quantity
NHS-LC-LC-biotin	Sigma Aldrich	B3295	10 mg
Lipofectamine 3000	ThermoFisher	L3000-001	1
Dulbecco's Phosphate Buffered Saline (D-PBS)	Gibco	14200-067	1
Fetal Bovine Serum (FBS)	Gibco	15140-122	1
15.5 µm Red fluorescent polystyrene microbeads (suspension)	Microparticles GmbH	PS-FluoRed-15.5	10 ml
15 µm FluoroMax green fluorescent polystyrene microbeads (dry powder)	Thermo-Fisher	35-48	5 g
ATTO 488 (modification: Streptavidin)	ATTO-TEC	AD 465-61	1 mg
ATTO 647N (modification: Streptavidin)	ATTO-TEC	AD 647N-61	1 mg
Hoechst 33342	Invitrogen	H1399	
Agarose powder			
Isopropanol (70%)			
Dimethyl sulphoxide			
Paraformaldehyde			
Deionized water			

Equipment Procedure I

Item	Supplier	Catalog Number	Quantity
Vortex mixer	VWR	444-0996	1
Centrifuge	Thermofisher	Megafuge 8R	1
Cell sorter	BD	FACSFusion	1
Safe-lock centrifuge 2 ml tubes	Eppendorf	0030120094	1
Ultrasonic cleaner	Branson	2800	1
Flexible clamps	VWR	USBE2680	1
Laboratory stand	VWR	241-0094	1
100 – 1000 µl micropipette	Eppendorf	3123000063	1
OneTip 100 – 1000 µl micropipette tips	Starlab	S1111-6811	1
Pipetteboy acu 2	Integra	155 016	1
Serological pipettes, 10 ml	Sarstedt	86.1254.001	1
Durapore® membrane filter, 5.0 µm pore size, hydrophilic PVDF, 25 mm	Merck	SVLP02500	1
Swinnex filter holder, 25 mm	Merck	SX0002500	1
Stainless steel tweezers Style 2A	VWR	OUTI2A	1
K6 Forceps, polybutene terephthalate	VWR	232-1313	1
Sterile syringe, Injekt®-F Solo 1 ml	VWR	720-2561	1
Ibidi glass bottom µ-dishes	Ibidi	81158	1
5 mL round-bottom polypropylene tube	Falcon	352063	1
15 ml conical centrifuge tubes	Thermofisher	339650	1
CellTrics strainer, 50 µm	Sysmex	04-004-2327	1
Accudrop fluorescent beads	BD	345249	1
CST beads	BD	656501	1

Equipment Procedure II

Item	Supplier	Catalog Number	Quantity
Kinematic mirror mount	Thorlabs	KCB1C	5
z-translation mount	Thorlabs	SM1Z	2
x-y fine translation mount	Thorlabs	ST1XY-D-M	1
x-y coarse translation mount	Thorlabs	CXY1A	1
Fluorescent filter cube	Thorlabs	DFM1B	4
Fluorescent filter inset	Thorlabs	DFM1T3	2
Corner mirror insert	Thorlabs	DFM1-M-P01	1
Filter wheels	Thorlabs	FW1A	2
Neutral density filter set	Thorlabs	NDK01	1
2D galvo system	Thorlabs	GVSM002EC/M	1
Galvo system mount	Thorlabs	GCM102/M	1
Objective nosepiece	Thorlabs	CSN500	1
1" round mirror	Thorlabs	BB111-E02	5
Confocal scan lens	Thorlabs	LSM03-VIS	1
Confocal tube lens	Thorlabs	TTL200-A	1
Camera tube lens	Thorlabs	AC254-075-A-ML	1
Relay lens 1	Thorlabs	AC254-040-A-ML	1
Relay lens 2	Thorlabs	AC254-050-A-ML	1
Fiber coupling lens	Thorlabs	AC127-019-A-ML	1
Aspheric condenser lens	Thorlabs	ACL2520U-A	1
Rectangular dichroic mirror	Thorlabs	DMLP567R	1

Long pass filter	Thorlabs	FELH0550	2
90:10 beamsplitter, rectangular	Thorlabs	BSX10R	1
Large core multimode optical fiber	Thorlabs	M96L02	1
Small core multimode optical fiber	Thorlabs	M65L02	1
Threading adapter for scan lens	Thorlabs	SM2A33	1
Threading adapter for ½" optics	Thorlabs	SM1A6	1
SMA fiber adapter plate	Thorlabs	SM1SMA	2
60 mm cage plate	Thorlabs	LCP08-M	2
30 mm cage plate	Thorlabs	CP36-M	5
30 mm cage plate, unthreaded	Thorlabs	CP33-M	1
30 mm to 60 mm cage adapter	Thorlabs	LCP33-M	2
Lens tube	Thorlabs	SM1L10	1
Dovetail adapter	Thorlabs	CSA1003	1
1.5" cage rods	Thorlabs	ER1.5	12
4" cage rods	Thorlabs	ER4	12
10" cage rods	Thorlabs	ER10	4
12" cage rods	Thorlabs	ER12	4
Post holder	Thorlabs	PH40-M	6
Post	Thorlabs	TR40-M	6
Sample stage	Thorlabs	MP100-MLSH	1
Sample holder	Thorlabs	MLS203P2	1
Illumination LED, far red	Thorlabs	M730L5	1
LED driver	Thorlabs	LEDD1B	1
USB camera	Thorlabs	DCC1545M	1
Motorized translation stage	Thorlabs	PLS-XY	1
Motorized vertical stage	Zaber	X-VSR-E	1
Piezoelectric objective scanner	Physik Instrumente	ND72Z2LAQ	1
Threading adapter (for objective scanner and Nikon objectives)	Physik Instrumente	P-721.11Q	1
DAQ	National Instruments	PCIe-6323	1
BNC breakout cable	National Instruments	BNC-2110	1
Line-scan camera	Teledyne e2v	EV71YO1CCL2210 - BB3	1
Line-scan trigger cable terminal	Teledyne e2v	OR-YXCC-27BE2M1	1
Frame grabber	Teledyne DALSA	Xtium-CL MX4	1
CCD camera	Andor	Newton DU940P-BV	1
Spectrometer, f=500 mm (300, 1200 and 1800 l/mm grating), 2 outputs	Andor	SR500	1
532 nm excitation laser	Coherent	Helios 532-4-125	1
642 nm excitation laser	Omicron	QuixX 642-140 PS	1
4x Plan Apochromat	Nikon	MRD70040	1
10x Plan Apochromat	Nikon	MRD70170	1
25XC Sil CFI Plan Apochromat	Nikon	MRD73250	1
Fluorescent microscope slide	FSK4	Thorlabs	1
30 mm cage system target	VRC26PT	Thorlabs	1
60 mm cage system target	LCPA2	Thorlabs	1
Iris diaphragm	SM1D12D	Thorlabs	2
Calibration slide, 1/10 and 1/100 mm	5916720	Bresser Optik	1
SM1 caps	CM1CP2	Thorlabs	3

Software

Item	Version
LabView	2017
NI DAQmax	2017
MATLAB	R2021a
Python	3.9.13
FIJI ImageJ	1.53t

Procedure I: Intracellular Lasing

Preparation of Polystyrene Microbead LPs ● TIMING 2-3 h

1   Add polystyrene LPs to a centrifuge tube. (This procedure was optimized using dry fluorescent polystyrene particles; specifically FluoroMax microbeads by ThermoFisher, which are available in green and red). The exact quantity of LPs is not crucial at this stage, but we typically begin with a number of LPs that exceeds the number of cells in the culture dish.

2   Optional: The fluorescence bioassay for uptake quantification requires coating the LP surface with biotin. For this, weigh and dissolve 1 mg of NHS-LC-LC-biotin in 100 µl Dimethyl sulphoxide (DMSO), sonicating the mixture if necessary to ensure that biotin dissolves completely.

    ! CAUTION Direct exposure to DMSO can cause skin irritation. Wear personal protective equipment including suitable gloves when handling DMSO, and work inside a chemical fume hood to prevent inhalation of fumes.

3   Suspend the LPs in 100 µl of DMSO or biotin/DMSO (for the fluorescent bioassay). Leave the mixture for 30 min.

4   Take the (biotin/)DMSO/LPs solution and add it to 1 ml deionized water (DIW).

    ▲ CRITICAL Ensure a ratio of DIW:DMSO of 10:1 or higher, otherwise the polystyrene beads will not sediment during centrifugation because the density of the solvent is higher than the density of the microbeads.

5   Vortex the solution for 5 s, centrifuge it at 500 G for 5 min, and remove the supernatant with a pipette.

    ? TROUBLESHOOTING

6   Wash the LPs 5 times. For each washing step, resuspend the LPs in 1 ml of DIW and repeat Step 5. After the last washing step, resuspend the LPs in 1 ml DIW to have a stock solution.

    ▲ CRITICAL Ensure the DMSO is completely removed during the washing steps. Remaining DMSO will later wash off the biotin, leading to unstained microbead lasers which appear as false positives in the uptake assay.

7   Add 10 µl/ml of Lipofectamine 3000 to the stock solution in DIW and vortex the solution for 5 s. Wait for 30 min.

8   Centrifuge the mixture at 500 G for 5 min and remove the supernatant.

9   Wash the LPs once with DIW and then refill the centrifuge tube with DIW to obtain a LP stock solution.

    ■ PAUSE POINT You can store the coated microbead lasers for a few hours before proceeding with the cell seeding; however, the best results are achieved when resuming immediately.

10   Centrifuge the LPs/DIW solution at 500 G for 5 min, remove the supernatant, and refill the centrifuge tube with cell culture medium.

Box 2 | Preparation of bespoke semiconductor LPs ● TIMING 1-2 h

1   The starting point of this procedure assumes that LPs have been defined and etched on a semiconductor wafer, leading to free-standing but adhering LPs on the surface of the wafer. Cleave the wafer to obtain a piece of wafer that can fit the opening diameter of the centrifuge tube.
    ▲ CRITICAL Handle the wafer with K6 style plastic forceps where possible. Physical damage to the wafer can lead to unwanted cleaving or formation of shards in the ultrasonic bath.
    ! CAUTION Many wafers contain toxic materials, which requires taking precautions for safe handling and disposal. The LPs themselves must not contain any toxic materials or else should be encapsulated to avoid compromising cell viability.
2   In the cell culture hood, sterilize the wafer piece with LPs by submerging it in ethanol for 10 minutes, then leave it in the cell culture hood for approximately 5 min to dry.
3   Insert the wafer piece into a sterile rounded-bottom 2 ml centrifuge tube with the surface containing LPs resting against the tube wall.
4   Add approximately 200 µl (or enough to entirely submerge the wafer piece) of cell culture medium to the tube, close the tube, and seal it with parafilm.
5   Using flexible clamps, place the tube in the ultrasonic bath and sonicate for 30 min.
    ▲ CRITICAL The tube should be positioned in the bath at an angle of approximately 45° such that the opening of the tube is above the water surface and the side of the wafer piece containing LPs is resting against the lower surface of the tube. We observed that the proximity to another surface during sonication greatly improves the efficiency and speed of the detachment of the LPs into the cell medium.
    ? TROUBLESHOOTING
6   Remove the tube from the ultrasonic bath and sterilize it with 70% IPA prior to placing it in the cell culture hood.
7   Carefully remove the wafer piece from the tube by using fine and sterile tweezers that can reach into the tube, e.g., stainless steel 2A tweezers.
8   To ensure the LPs have been removed, wash the wafer piece in ethanol and inspect the surface. Any iridescence or hue (typically visible to the naked eye for periodic structures including patterned and etched LPs) should no longer be present and the surface should be reflective.
    ? TROUBLESHOOTING
9   Sterilize the single-use filter membrane by dipping it in ethanol and leaving it in the cell culture hood to dry for 5 min.
10 Unscrew the two parts of the sterile filter holder, insert the filter membrane on top of the rubber ring, and close the filter holder again.
11 Fill approximately 1 ml of cell culture medium into a sterile syringe. Pass the cell medium through the assembled filter into a separate tube for waste collection. This wets the membrane filter prior to filtration of the LP suspension.
12 Fill the syringe with the suspension of LPs in cell culture medium and pass the suspension through the filter into a new tube for LP collection.
13 Recover remaining LPs that may have adhered to the surfaces of the original tube or the filter. To achieve this, pipette 200 µl of cell culture medium into the emptied tube, sonicate the tube for 1 min, and pass this suspension through the filter into the LP collection tube. The final concentration in the LP stock solution can be estimated from the size of the wafer piece and the density of LPs on its surface. If the protocol is successful, the loss of LP during the cleaning and filtration steps should be well below 50%.

Adding LPs to Cells ● TIMING 1 h

11 Determine the necessary volume of LP suspension needed, based on the concentration of LPs in the stock solution, the number of cells in the dish, and the desired ratio of LPs to cells. LPs can be counted on a hemocytometer to quantify the efficiency of the LP preparation workflow and to determine the necessary volume for the desired ratio of LP to cells.
12 In the cell culture hood, remove the medium from the cell culture dish and wash the cells once with PBS.
13 Add the suspension of LPs in cell medium. If necessary, top up the cell culture dish with more medium.

? TROUBLESHOOTING

■ **PAUSE POINT** Once the LPs are settled to the bottom of the cell culture dish (typically after a few hours), the cells will begin internalizing the LPs; the speed of the uptake will depend on the cell type and the size and geometry of the LPs.

14 Wait for the uptake of LPs (we usually leave the sample overnight to allow settlement and uptake of the LPs). Should additional media changes be required, they must be performed very carefully, as this might wash away non-internalized LPs.

▲ **CRITICAL** The timing of Steps 12-14 may require further optimization when working with different types of cells or LPs. For small (< 3 μm diameter) LPs, the LP suspension can alternatively be added during splitting and re-seeding of the cell culture. Methods of assessing internalization of the LPs are described in the following sections and should be used during optimization of the LP internalization workflow.

? TROUBLESHOOTING

Fluorescence Microscopy Bioassay ● **TIMING** 2-3 h

15 Prepare the dye solution by mixing 20 μl of ATTO 488-streptavidin stock (1 mg/ml) and 10 μl Hoechst 33342 (2 mM) with 1 ml cell culture medium. The cell-impermeable ATTO 488-streptavidin conjugate selectively binds to the biotin coating of the non-internalized microbead LPs, therefore it can be used as a marker for internalization.

▲ **CRITICAL** The emission spectrum of the dye used to label non-internalized LPs must be well separated from the emission of the LP itself (peak separation > 100 nm) to limit bleed-through of the very strong signal of the LPs into the spectral channel used to assess internalization. We recommend ATTO 488-streptavidin for red fluorescent LPs and ATTO 647N-streptavidin for green fluorescent LPs.

16 Remove the cell culture medium from the cell culture dish with the LPs, add the dye solution to the cells, and incubate for 15 min.

▲ **CRITICAL** Perform all washing steps very carefully and slowly to avoid washing away non-internalized LPs.

17 Remove the dye solution and wash the cells once with PBS.

18 Add 1 ml Paraformaldehyde (PFA, 4% in PBS).

! CAUTION Exposure to PFA can have toxic and carcinogenic effects. Handle PFA in a fume hood, wearing protective equipment including suitable gloves, to avoid skin exposure and inhalation. Use separate equipment (i.e., pipettes, glassware) for handling PFA and ensure appropriate disposal of contaminated waste.

19 After 15 min, remove the PFA and wash the cells three times with PBS, then refill with PBS. Close the culture dish and seal it with parafilm.

■ **PAUSE POINT** The fixed and stained cells can be stored in a 4°C fridge until imaging is performed.

20 On a fluorescence microscope, image all LPs using their intrinsic fluorescent signal.

▲ **CRITICAL** Image large FOVs with enough LPs for statistical analysis. Ensure excellent image quality of the two LP channels, easing the use of automated tools for particle counting (e.g., the FIJI ImageJ[51] measuring function).

21 Image the non-internalized microbead lasers in the same field-of-view (FOV) by recording signal from non-permeable ATTO488-streptavidin or ATTO647N-streptavidin signal.

22 The cells can be co-localized by imaging the Hoechst signal, or from phase-contrast images (Figure 4a).

## Fluorescence-Activated Cell Sorting (FACS) ● **TIMING** 0.5 d

23 For cell sorting by flow cytometry, prepare the following samples: i) the cell culture labelled with LPs, ii) a control sample of identical cells without LPs, iii) a sample of just LPs in suspension.

24 Detach the cells following the standard procedure applicable to the cells used and resuspend the cell pellet in FACS buffer (DPBS containing 2% FBS).

▲ **CRITICAL** Transport to external flow cytometry core facilities can either be done prior to or following dissociation, depending on the cell type. Cell transport might require designated bio-safety containers, depending on local regulations and cell type.

25 Filter the cell suspension through the 50 μm cell strainer to remove cell clumps and collect the filtered cell suspension into the 5 ml polypropylene tube.

26 Sort the cells (Figure 4b, Supplementary Figure 4) and collect the sorted cells in a centrifuge tube containing cell culture medium. (See Supplementary Figure 5 for exemplary measurement conditions and a gating strategy of the cell sorter).

▲ **CRITICAL** When designing the sorting conditions, account for the increased size of LP-containing cells, as well as the high brightness of the LP emission compared to conventional fluorescent labels.

27 Seed the sorted cells into an appropriate dish for imaging and leave in the incubator until the cells have attached. Following attachment, the cells can be imaged for additional control of internalization (e.g., with confocal microscopy, Figure 4c), or monitoring cellular uptake by refractive index sensing (Figure 4d), and hyperspectral confocal imaging of the LPs can be performed (Procedure II).
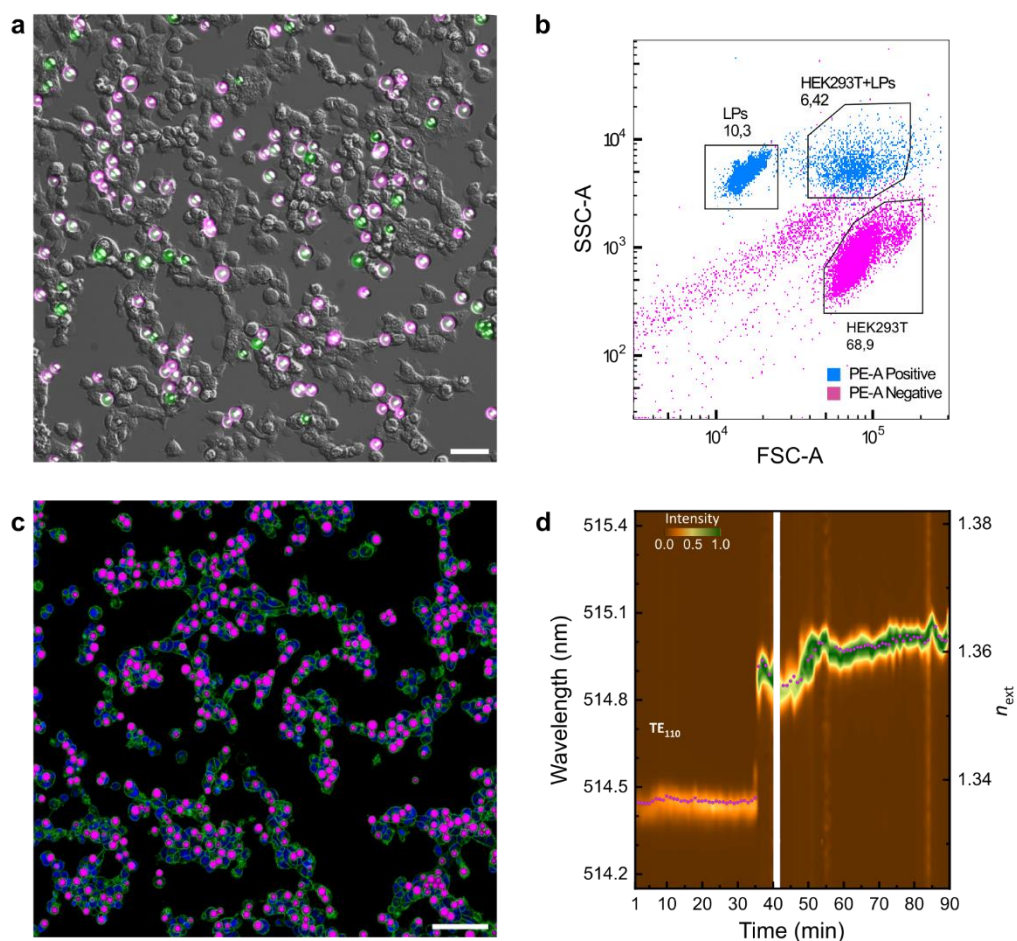
Figure 4 Controlling internalization of LPs. a, Fluorescence bioassay for green microbead lasers showing non-internalized (magenta) and internalized (green) LPs. Non-internalized LPs show green emission from the LP itself and magenta emission from the cell-impermeable ATTO 647N-streptavidin bound to their surface. Internalized LPs only show their intrinsic green emission. Scale bar, 50 μm. **b**, Flow cytometry scatter plot, sorting live singlet cells into populations with (blue) and without (magenta) internalized LPs. The color-coding corresponds to the intensity of the Rhodamine (PE-A) signal used to identify red fluorescent LPs. Numbers indicate the percentage of the different populations with respect to the total number of recorded events. **c**, Confocal x-y maximum intensity projection of the LP-positive (15 μm red fluorescent LPs, magenta) population of HEK293T cells, labelled with Hoechst (blue) and membrane-bound EGFP (green). The cells were re-seeded after cell sorting and imaged 12h later. Scale bar, 100 μm. **d**, Monitoring cellular uptake by measuring lasing spectra (brown-green colormap, left axis) for 90 min with two consecutive acquisitions. The refractive index (magenta circles, right axis) extracted from the spectra increases rapidly during cellular uptake of the LP at ca. 35

Procedure II: Microscopy and Spectroscopy

PC Setup and Installation ● TIMING 1 d

1   Insert the National Instruments DAQ board and Frame Grabber boards into open PCIe x16 slots in the PC.
2   Download and install the following commercial software programs and drivers from the respective manufacturers or from the data storage devices included with the equipment delivery: LabView, NI MAX, Thorlabs ThorCam, Andor Solis (or equivalent spectrometer software), GenICam CommCam, Teledyne Octoplus Software, and the Physik Instrumente PI Stage control software along with its LabView Drivers.
3   Request access to our hardware repository to download the custom-built applications GPScan.vi[52], NewGPScan.vi, ConfocalHyperspectral.exe and SapGUI.dll .
4   Create a working directory at a preferred location on the C drive (C:) and place ConfocalHyperspectral.exe and SapGUI.dll in this folder. For convenience, create a desktop shortcut to ConfocalHyperspectral.exe.
5   For data analysis, install MATLAB and Python with the open-source Python modules napari[53] and Trackpy[54].
6   Download 'GatherLab/sphyncs.zip'[55] and place the files in your data processing directory.

Construction of the Confocal Scanning ● TIMING 1 d

7   Start assembly of the microscope body (Figure 5) by placing the optical elements on the surface of the optical table. (Refer to CAD File {data repository DOI to be added upon formal acceptance}, Supplementary Table 1, Supplementary Note 1, and Supplementary Figures 1 and 2a for more detail on placement of the optical components.) The optical height of the beam path should be fixed at the height of the excitation laser beam. If this is impractical due to spatial constraints, one can first use a periscope or a pair of corner mirrors to raise or lower the beam height, making sure it remains horizontal.
    ▲ CRITICAL The distance along the optical axis between components where the beam is collimated is not critical, but it is recommended to keep it small where possible. Some components require precise positioning in z and should already be placed roughly in the correct position using a ruler: The spacing of the scan lens (L1) and the confocal tube lens (L2) must be equal to the sum of their respective focal lengths, the camera tube lens (L3) and the fiber coupling lens (L4) must be positioned such that their focus coincides with the camera (CAM1) and the optical fiber mount, respectively.
8   Power on the PC and the linear power supply unit for the motors of the galvo scanner.
9   Open LabVIEW and confirm that there is communication between LabVIEW and the DAQ.
    ? TROUBLESHOOTING
10 Using LabView, set the voltage applied to the galvo mirrors to 0V on both axes to ensure the galvo mirrors are centered prior to beginning alignment. One way to center the galvos is opening the NewGPScan.vi script, setting the 'VoltageFactors' to 10e-5, and running the script.
    ▲ CRITICAL The galvos need to be centered ('nulled') prior to starting alignment to ensure that the actual center of the confocal scan is aligned to the optical axis.
11 Turn on the excitation laser. Using the first pair of kinematic mirrors (KM1, KM2), center the beam in the cage system located on the side of the galvo mirrors that faces the laser. To ensure the beam path is not angled, select two positions (e.g., just before FC1 and just before GM) and confirm that the beam is centered at both positions, using the 30 mm cage system alignment target.
    ! CAUTION Avoid eye exposure to direct or reflected laser beams. Reduce the laser power during alignment and adhere to laser safety precautions including wearing appropriate eye protection. Any open exit apertures of filter cubes in the cage system should be closed off with SM1-threaded caps to block back-reflections.
12 Evaluate the profile of the excitation beam at the exit of the 90:10 beamsplitter cube located underneath the objective (FC2). Confirm the excitation beam gets collimated by L2, either by using a shearing interferometer, or by placing an iris aperture at different distances from the filter cube to check that the diameter of the excitation beam does not change with distance.
13 If necessary, manually move L2 in its mount along the rails of the cage system with the locking screws open until the beam is collimated.
14 Lock the mount holding L2 into place on the rails of the cage system and close the unused opening of FC2 with an SM1 cap to block the transmission of the excitation beam through the 90:10 beamsplitter.
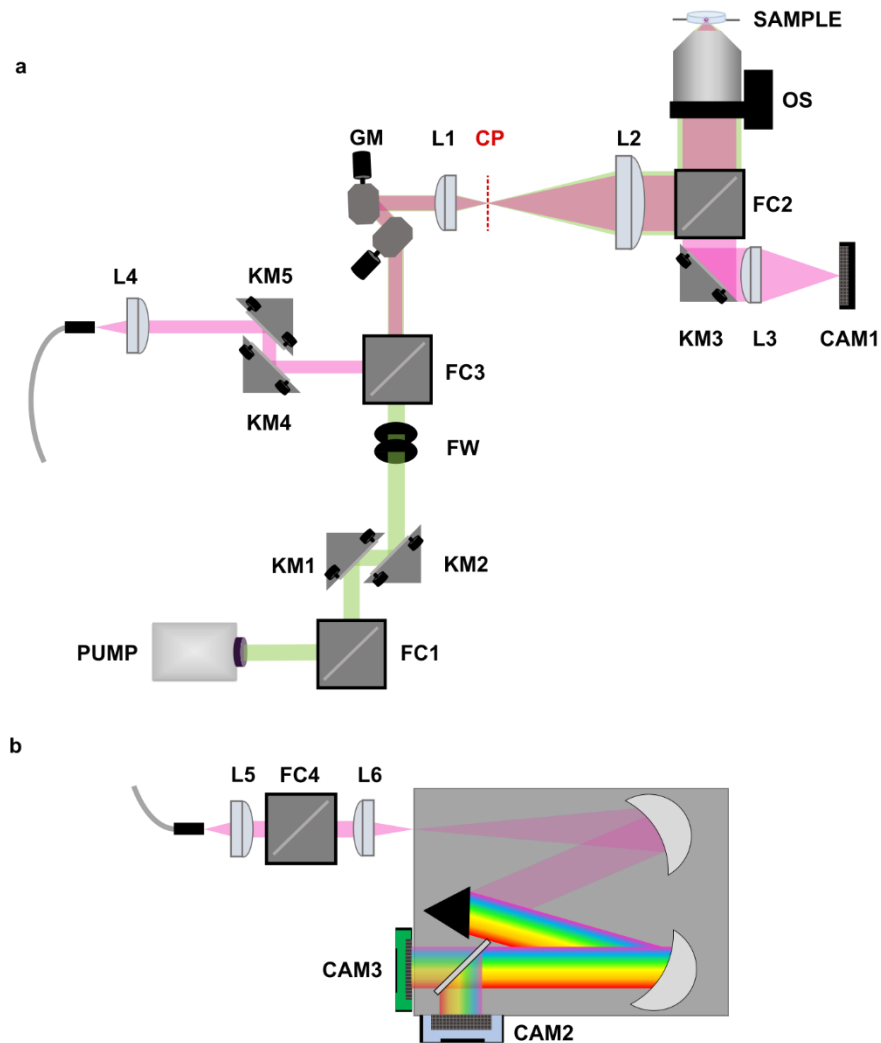
Figure 5 Microscope Overview a, Confocal scanning system. The main excitation laser (PUMP, green path) is aligned with two kinematic mirrors (KM1, KM2) and a filter cube (FC1) allows coupling of additional laser lines. The excitation can be attenuated with neutral density filters (FW) before it is passed to the 2D scanning galvo system (GM). The beam is expanded by the scan lens (L1) and confocal tube lens (L2) to overfill the back aperture of the objective, which is mounted on a piezo-electric objective scanner (OS) for optical sectioning. A 90:10 beam splitter (in FC2) and the imaging tube lens (L3) allow to obtain transmission microscopy images of the sample on a USB camera (CAM1). Emission from LPs in the sample (SAMPLE, magenta path) is collected by the objective, de-scanned by the galvo system, split off the excitation path by a dichroic mirror inserted into filter cube (FC3), and subsequently coupled into an optical fiber, using another set of kinematic mirrors (KM4, KM5) and a coupling lens (L4). **b**, Spectroscopy module. The signal emerging from the far end of the optical fiber is projected onto the slit plane of the spectrometer using a relay lens system (L5, FC4, L6). After passing through the spectrometer, the wavelength-dispersed signal can be read either on a CCD camera (CAM2) or the high-speed line-scan camera (CAM3).

15 Place the 60 mm cage system alignment target in the conjugate plane (CP) between scan and tube lens (the position where the spot size of the excitation beam is smallest) to evaluate the beam position for aligning the galvos to the image center.

16 Loosen the locking screws on both galvo mirrors and manually align the galvo mirrors by gently rotating the motors within their mounting holes until the excitation spot is centered.

17 Place the alignment target just before L2 to center the spot at this position, performing fine adjustments with KM1 and KM2 if needed.

18 Iterate between Step 16 and 17 until the beam is centered at both positions before fixing the lock screws of the galvo mirrors.

19 Optional step: To couple additional laser lines, other inputs of filter cube FC1 can be used. A kinematically locked corner mirror can be inserted in FC1 to allow switching between the different excitation paths. A separate pair of kinematic mirrors should be included on the laser-facing side of FC1 for the alignment of

each additional laser. Only this additional pair of kinematic mirrors should be used to center the additional beam at the alignment positions previously described.

Alignment of the Detection ● TIMING 2-3 h

20 For alignment of the camera, start with a low-magnification air objective and a relatively thick fluorescent sample, e.g., a fluorescent microscope slide. Put the fluorescent sample onto the sample holder.
▲ CRITICAL Using a fluorescent sample that is much thicker than the depth of field of the objective ensures that the alignment is independent of the positioning of the sample.
! CAUTION Placing the fluorescent sample at the focus of the excitation laser beam will cause reflection from its surfaces. An image of this reflection is formed on the camera, which can cause damage to the camera chip. Ensure this reflection is blocked by a suitable bandpass filter (LP1) before proceeding.

21 Move the fluorescent sample into the focus of the excitation laser, using the motorized stage in z. First estimate the position of the focus from the working distance of the objective, and then readjust the sample position until a fluorescent spot generated by the excitation beam is visible within the sample by naked eye.

22 Turn on the ThorCam software to connect to the Brightfield camera (CAM1) and display a live image.

23 Manually move the camera tube lens (L3) until the image of the fluorescent spot is in focus, i.e., the spot size in the image is minimized.
▲ CRITICAL STEP Camera CAM1 will later be used for navigation and positioning of samples into the confocal scan field, as well as for the alignment of the confocal detection fiber. Misalignment of CAM1 will make it more difficult to image the correct regions of interest, and any misalignment will likely propagate to the other components. Here, we align the image plane of the camera to the focus of the excitation laser, whose position may be wavelength-dependent due to the possibility of chromatic aberration in the system. Therefore, we recommend performing this step whenever switching between excitation lasers of substantially different wavelengths.

24 Use the kinematic mirror (KM3) to center the spot in the image.

25 For alignment of the confocal detection, the image needs to be focused on the lower surface of the fluorescent slide in the brightfield image. Move the sample in z until the surface structure on the fluorescent slide and the confocal excitation spot are both focused sharply.

26 Visualize the collection path with light coupled into the other end of the optical fiber, e.g., by mounting the fiber face in front of the Brightfield LED or another light source with a wavelength suitable for following the collection path. If using multiple fibers for detection, start with the fiber with the largest core.

27 Place the 30 mm cage system alignment target behind KM5, facing the coupling lens L4, to evaluate the light emerging from the fiber backward along the collection path.

28 Use the kinematic mount of the fiber to center its output on the alignment target.

29 Manually slide L4 along the cage system to collimate the light emerging from the fiber.
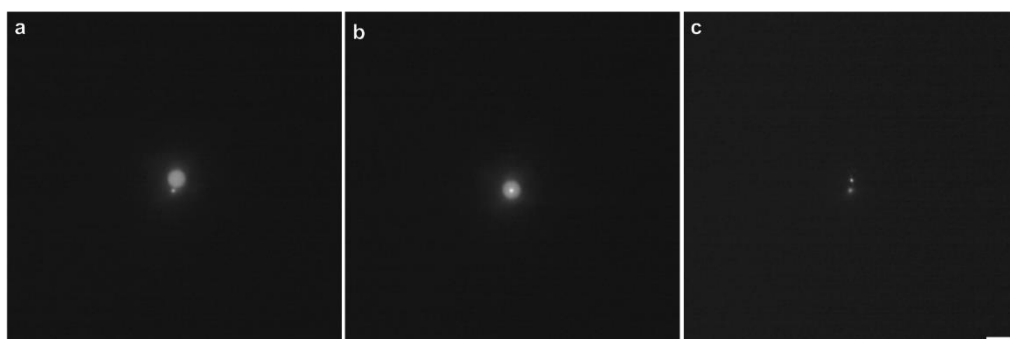
Figure 6 Coarse Pinhole Alignment. Assessing the alignment of the pinhole by comparing the reflection of light emerging from the 105 µm fibre (large spot) and fluorescence from the confocal excitation (small spot), **a**, misaligned and **b**, aligned, i.e., concentric. **c**, Reflected signal from a misaligned 10 µm fibre (upper spot) with a diameter comparable to the size of the excitation spot (lower spot). Scale bar, 25 µm.

30 Remove the alignment target and adjust the power of the excitation laser and the light coupled into the fiber such that they form spots of similar brightness on the camera (Figure 6a).

31 ▲ CRITICAL STEP Minimize the size of the spot formed by the light emanating from the fiber by fine-adjusting L4 with its z-translation mount. For this, it is crucial that the focus of the camera is on the lower edge of the fluorescent slide, such that the fluorescent spot generated by the excitation beam and the reflection of light from the fiber are in focus simultaneously. The image formed by the output of the fiber represents the collection spot and is an indication of the pinhole size. For large fibers ('open pinhole'), the spot size exceeds the size of the confocal excitation spot (Figure 6a,b), whereas for small core sizes ('closed pinhole'), the spot sizes are comparable (Figure 6c).

32 ▲ CRITICAL STEP Walk the beam of the collection path, using the two kinematic mirrors KM4 and KM5, such that the two spots are concentric (Figure 6b).

33 Toggle the sample position along z and ensure the image of the output of the fiber defocuses homogenously and symmetrically to check for any angles in the detection path. To eliminate angles, iterate between defocused and focused images and adjust KM4 and KM5 until both images are concentric.

Camera Configuration and Alignment ● TIMING 1 d

34 Turn on the line-scan camera CAM3 and the HyperspectralConfocal and the GenICam camera software programs, as well as the NewGPScan.vi and the galvos.

35 In the HyperspectralConfocal software, set the number of points in x and y to 20 and the acquisition time to 199 µs.

36 In the GenICam software, connect to the correct frame grabber board and camera and load the parameter textfile (params.txt in the directory of the HyperspectralConfocal software) into the 'hyper terminal'.

37 Increase the number of frames in the HyperspectralConfocal software to a larger number, e.g., 100. Should a different camera model and/or software than those listed in the materials section be used, connect the camera to the PC and configure the acquisition to display the recorded frames in real-time, using a short camera refresh rate of e.g., 10 fps.

38 Turn on the camera CAM2, which is connected to the other output port of the spectrometer and start the software controlling CAM2. If the spectrometer has only one output port, dismount the line-scan camera (CAM3) and mount CAM2. Set the readout for CAM2 to imaging mode and set the grating of the spectrometer to reflection mode (often referred to as '0 nm' in the control software).

39 Place a homogenous, scattering object (e.g., a white piece of paper) in front of the entrance slit of the spectrometer to produce an image of the slit on camera CAM2. Remove the scattering object.

40 Note the pixel number along x where the image of the closed slit is formed. (We will use the following convention to describe the spatial axes: z – along the beam path; y – perpendicular to the beam path, vertical direction; x – perpendicular to the beam path, horizontal direction, which corresponds to the direction of spectral dispersion in the spectrometer).
    ? TROUBLESHOOTING

41 Assemble the cage system for the fiber relay system, at this stage not yet connecting it to the spectrometer and not yet mounting lens L6. FC4 is left empty at this stage but can later be used to relay alternative signals to the spectrometer, or to couple light into the optical fiber with a mirror during the alignment procedure.

42 Coarsely position L5 one focal length away from the fiber adapter plate using a ruler.

43 Turn on the microscope illumination LED until the light following the detection path and emerging from the optical fiber at the spectrometer side forms a spot that can be seen by naked eye.

44 Manually slide L5 along the cage system until the light emerging from the fiber is collimated by L5 and fix its position.

45 Add L6 to the relay system and mount the relay system on the input side of the spectrometer, with L6 roughly positioned such that its focus sits in the plane of the spectrometer entrance slit.

46 If the spectrometer used does not have a cage system adapter, manually pre-align the relay system to the spectrometer slit in x-y, avoiding any tilts of the optical axis of the relay system with respect to that of the spectrometer.

47 Fully open the slit of the spectrometer to display an image of the fiber core on the CCD camera, using the signal from the illumination LED transmitted through the fiber.

48 Move L6 first manually, then with the z-translation mount, to focus the image of the fiber core on CAM2.

49 Adjust the x-y-translation mount of the fiber next to L5 such that the image of the fiber core on the camera is centered along y and positioned at the pixel value corresponding to the position of the closed slit noted in Step 40.

50 With CAM2 now available to accurately detect light emanating from the fiber, the coupling of light from the microscope into the fiber should be aligned more precisely. To achieve this, set the spectrometer grating to a wavelength within the emission spectrum from the used fluorescent target, switch CAM2 to spectral readout, and close the spectrometer entrance slit to a standard measurement setting, e.g., 30 μm for Andor Shamrock spectrometers.

51 Mount the fluorescent slide on the sample holder and turn on the excitation laser.
! CAUTION Reflections of the excitation laser can damage the spectrometer and the connected cameras. Always ensure the spectrometer is protected by a suitable bandpass filter (LP2).

52 Fine-adjust the fiber coupling optomechanics of the confocal detection (KM4, KM5, L4) to maximize the intensity of the fluorescence measured on the camera.

53 Select settings for the grating (type and position) such that the fluorescence signal is as horizontal as possible and equal in brightness on either side of the camera and save a reference spectrum.

54 Switch to the alternate output port in the spectrograph settings to divert the signal to the line-scan camera (CAM3), or, if your spectrometer does not have two output ports, dismount CAM2 and mount the line-scan camera.

55 Optional: If you need to dismount CAM2, acquire the reference spectra needed for the spectral calibration in Step 75 before proceeding.

56 To configure the detection for the next alignment step, set the grating back to reflection mode and set the spectrometer shutter to 'Open'.
▲ CRITICAL The line-scan camera does not trigger the spectrometer shutter; therefore, it must be kept in the 'Open' setting whenever using the line-scan camera.

57 In the HyperspectralConfocal software, click on 'Acq Spectrum' and then run the LabView scan (by pressing the run arrow, and then 'Raster Scan') to continuously display a live spectrum (see Supplementary Figure 6 for an exemplary screenshot of the GUI).

58 Adjust the fiber translation mount next to L5 along y until the brightness of the central peak, corresponding to a 1D image of the fiber, is maximized.
? TROUBLESHOOTING

59 Adjust the position of the line-scan camera (see Supplementary Figure 7 for the camera flange we designed) in the z-direction to focus the peak (i.e., maximizing brightness and minimizing the width of the 1D image of the fiber on the camera).

60 Move the camera in x such that the peak is centered on the detector.

61 Set the grating back to the settings used for the reference spectrum in Step 53.

62 Continuously acquire spectra and (slightly) rotate the line-scan camera until the brightness of the fluorescence is homogenous across the detector (or as similar to the shape of the reference spectrum (Step 53) as possible) .
With the grating again in reflection mode, check the alignment (x-y-z) of the line-scan camera and, if needed, re-align the camera without rotating it.
▲ CRITICAL Misalignment of the line-scan camera will negatively impact the spectral quality and signal-to-noise ratio of subsequent measurements. The camera or the relay might require realignment when switching to a different grating.

63 Fix the lock screws on the camera adapter and adjust the y-position of the fiber mount for maximum signal one more time.

Calibration and Test Image Acquisition ● TIMING 0.5 d

64 Mount the calibration slide on the sample holder and navigate to an area with clearly marked distances for spatial calibration.

65 Bring the pattern into focus on CAM1 and save a transmission brightfield image.

66 Configure the detection such that the transmitted light from the LED reaches the line-scan camera with the spectrometer grating set to reflection mode.

67 Adjust the brightness of the LED such that it produces a clear and bright, but not saturated peak in the live spectrum displayed in NewGPScan.vi.

68 Set the galvo voltages in the HyperspectralConfocal software 'Scanning Setup' menu to ±50 V, the number of pixels in x and y to 400, the number of z-steps to 1, and the number of frames to 3. Confirm that the voltage factors in the LabView script are set to 0.1 (which will lead to an absolute applied voltage of ±5 V).

69 Record an image sequence by clicking 'RecordRAM' in the HyperspectralConfocal software, followed by 'Raster Scan' in NewGPScan.vi.

70 Click on 'Conv Seq' to batch-convert the 3 images. The converted images can be found in the directory of the HyperspectralConfocal software. They consist of two panels, both representing the raw image, one with color-coding for dominant wavelength and one with color-coding for intensity. The pattern of the calibration slide should be visible in these images (Supplementary Figure 8).

? TROUBLESHOOTING

71 To save the image data, first click on 'Save One' and select a destination folder and name for the dataset. By clicking 'Save Seq', all image buffers will be saved to the destination folder as separate, numbered image files (e.g., 'DataName_frame00000.tif').

72 Load the processed images into your preferred image processing software to determine the actual physical size of the ±50 V scan field and make a note of this value. One can later input this value into the open-source processing functions (Procedure II, Stage 3) for accurate spatial calibration. As expected, the scan field size scales with objective magnification (Supplementary Figure 9), but we recommend repeating the calibration for all objectives that are used on the system routinely.

73 Mount the spectral calibration lamp in the space between KM5 and L4 to couple its signal into the detection fiber.

74 Set the center wavelength of the spectrometer grating to a value that lies within the expected emission range and set the spectrometer output to CAM2.

75 With the spectrometer slit closed to the minimum value, measure the spectrum of the calibration lamp on CAM2.

76 Then set the spectrometer output to the line-scan camera. With the live spectrum displayed in LabView, verify that the current acquisition parameters provide sufficient signal-to-noise ratio to clearly locate the peaks; increase the acquisition time or brightness of the calibration lamp if needed.

77 Acquire and save images of the spectra on the line-scan camera for later processing. Repeat this procedure for each grating that is regularly used on the system.

▲ **CRITICAL** The spectral calibration is crucial for obtaining accurate measurements, particularly for the calculation of absolute refractive index from the measured spectra. Ensure the measured calibration spectra contain at least 3 well-defined peaks (Supplementary Figure 10).

LP Reference Measurements ● TIMING 2-3 d

78 Prepare two samples for the reference measurements: A suspension of LPs in a medium of well-known, homogenous refractive index and a 3D dispersion of LPs (e.g., LPs in DIW and agarose, Box 3). For our benchmarking and reference measurements, we use FluoRed LPs, which reliably generate lasing spectra of good quality, offer homogenous lasing thresholds of around 0.5 nJ/pulse (Supplementary Figure 11) and emit spectra with resolution-limited lasing peaks. (They are not compatible with Procedure I; therefore, we recommend using dry FluoroMax LPs for experiments requiring intracellular integration).

Box 3 | Preparation of Reference LP samples

1 Preparation of beads in DIW
   i.   Pipette 15 µl of the FluoRed stock solution into an ibidi imaging dish.
   ii. Add 1-2 ml of DIW and gently swirl the dish to homogenously distribute the LPs.
   iii. Close the dish and seal it with parafilm.
2 Preparation of a 3D dispersion of beads in agarose

---

79   Keep the excitation beam stationary and configure the detection for displaying a live spectrum in the spectral range of emission from the used LPs, either on the CCD camera (CAM2) or on the line-scan camera (CAM3). For collecting spectra with the line-scan camera, run the continuous spectral acquisition with LabView and set the 'voltage factors' to 10e-05 to keep the beam stationary.

80   Visualize the position of the laser beam on the USB camera image (CAM1), e.g., with a fluorescent sample, and mark it with the drawing tool in the ThorCam software. This will ease the positioning of the LPs in the next step.

81   Mount the sample containing LPs suspended in DIW.

82   By moving individual LPs into the excitation spot and observing their spectra, identify a combination of excitation pulse power and pixel dwell time that leads to lasing spectra of good quality. Using pulse energies approximately 5- to 10-fold above the lasing threshold, and scan rates ca. 5-fold slower than the repetition rate of the excitation laser is a good starting point. It is expected that a stationary beam with a typical pulse repetition rate suitable for fast scans will bleach many types of LPs much more quickly (even within seconds) than the continuously moving beam used during scanning measurements.

83   Acquire an x-y-t sequence of images of the DIW sample, following the same workflow as Steps 68-71. (If the 'voltage factors' were decreased in Step 79, set them back to 0.1 for correctly calibrated scan fields.)

84   Use the 'Conv One' function to check image sharpness and signal-to-noise ratio.

85   Save the image sequence for later processing, including calibration of the refractive index sensing script.

86   Repeat Steps 83-85 for a range of acquisition parameters to compare how different conditions affect the quality of images. Exemplary images we obtained at different scan speeds (e.g., 25 kHz, Figure 7a; 125 kHz, Figure 7b) are included, as well as an example of displaying the results color-coded by wavelength (Figure 7c). The collection efficiency will vary for different objectives (Figure 7d). To assess the signal-to-noise ratio, evaluate the quality of individual spectra (Figure 7e,f) rather than just the intensity-processed images.

? TROUBLESHOOTING

87   Connect to the piezoelectric objective scanner (PIStage) through LabView by enabling the 'stage on' button, running the script and clicking 'Connect'. Once you confirm the connection in the pop-up window, the stage will initialize.

! CAUTION The PIStage will move during its initialization for axis referencing. Ensure there is no physical obstruction within the travel range of the objective mounted on the PIStage since collisions could damage the objective or the PIStage.

88   Mount a 3D LP sample on the sample stage, e.g., the dispersion of LPs in agarose.

89   Set up the z-scan by entering a step size (as negative value, in nm) and stack size (as number of slices) in the HyperspectralConfocal software. The 1%w/v agarose matrix is sufficiently transparent so that the imaging parameters established in Steps 82-86 should not require readjustment.

90   Acquire and save the stack. Assuming the objective scanner is turned on, and the stack height and step size have been defined, stacks are acquired automatically by following the same acquisition routine from the x-

y-t sequences before. If both the 'frame number' and the 'number of slices z' are > 1, an x-y-z-t sequence is acquired.

? TROUBLESHOOTING
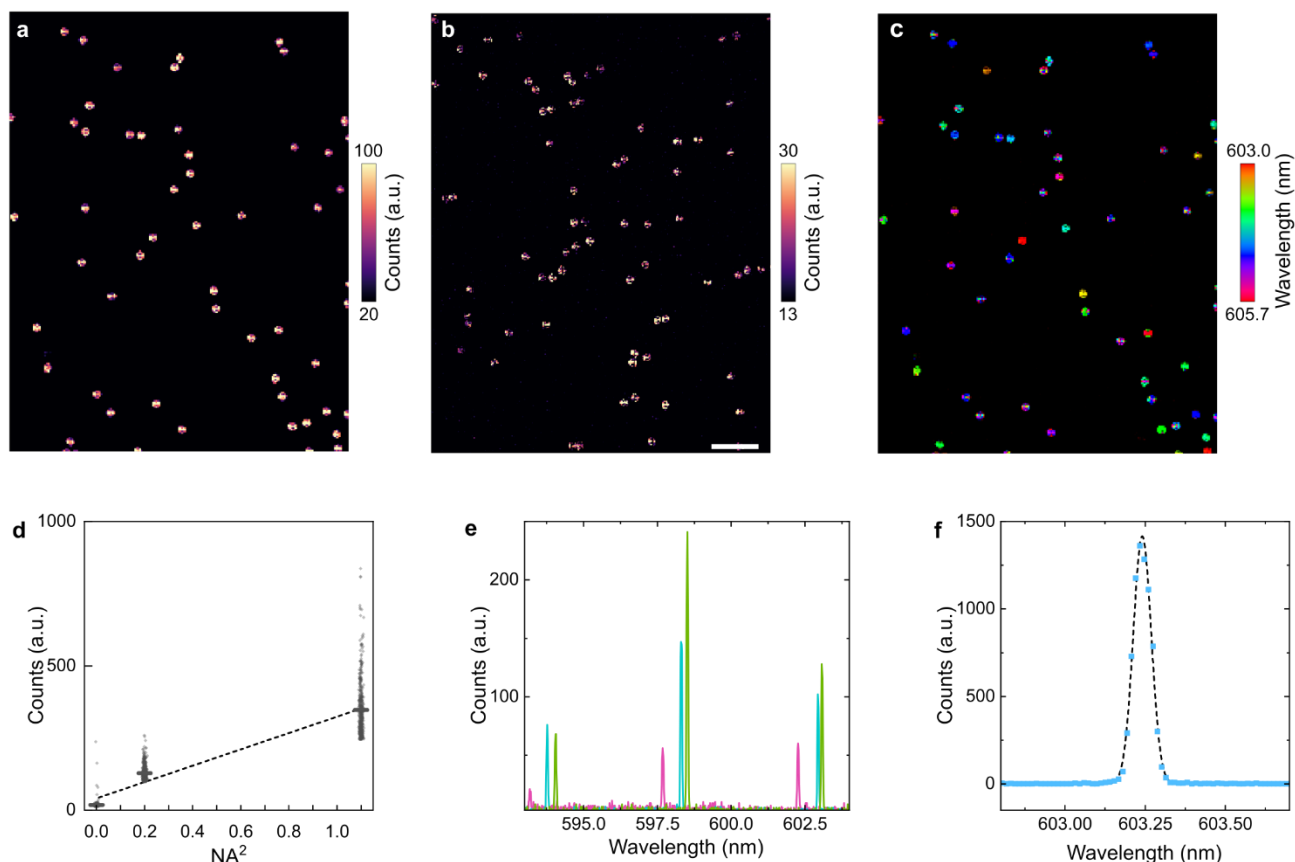
Figure 7 Typical results of reference measurements. a, Hyperspectral confocal images of FluoRed polystyrene bead LPs at 25 kHz and **b**, at 125 kHz, color-coded by intensity. Scale bar, 100 μm. **c**, Hyperspectral image from a, color-coded by wavelength of the central lasing peak. **d**, Comparison of measured peak intensities with three different objectives, showing a linear relationship between the average spectral brightness and the solid angle of collection of the objective, which is given by the square of its NA. **e**, Typical spectra of FluoRed microbead LPs, extracted from 3 different LPs from the image shown in a. **f**, Resolution-limited lasing peak from FluoRed lasing spectrum, measured with single-pulse excitation (125 kHz scan rate). Experimental data (blue squares) and gaussian fit (dashed black line) indicating a spectral FWHM of 0.06 nm, equivalent to the nominal resolution of the spectrometer used.

Acquisition of Experimental Data ● TIMING 2-3 h

91 Prepare a sample, referring to Procedure I for cell seeding and LP integration.
    ▲ **CRITICAL** Depending on the desired FOV size, optical resolution, and collection efficiency, you might use an immersion objective. When selecting cell culture dishes for imaging, account for compatibility of the dish with the immersion medium.

92 Select imaging parameters for the acquisition. It is important to have prior knowledge of the signal-to-noise ratio of images and spectra for the type of sample and LP to understand the minimum pixel dwell times required for the desired image quality. Additionally, technical limitations and requirements need to be taken into consideration (Box 4).

Box 4 | Choosing Acquisition Parameters
1 Pixel dwell times ≥ 8 μs are supported by the camera configuration.
2 The size of each voxel in x-y should not be larger than half of the diameter of the LPs to avoid under-sampling.
3 The size of voxels in z can be larger when measuring with the 'open pinhole' fiber and a low-NA objective, but the image of an individual LP should span at least two z-slices.

4	Reducing the number of pixels in x increases the scan speed for a given spectral acquisition rate, thereby increasing the speed of the faster-moving galvo. The galvo has a maximum line rate of 175 Hz; therefore, faster spectral acquisition rates require additional pixels in x (at least 715 pixels in x at 125 kHz, 571 pixels in x at 100 kHz, etc.).
5	For large measurements, such as x-y-z-t scans, the duration of continuous scans might be limited by the availability of RAM, since the image buffers are held in the RAM until the data is saved by the user. If this is a limiting factor, the active area of the camera can be cropped to read out only the centermost pixels by setting the camera width to a user-defined value in the HyperspectralConfocal software.
6	Due to the camera communication settings, the camera width needs to be an integer multiple of 4. After changing the camera width, re-load the parameter file into the GenICam CommCam software through the hyper terminal.
7	In dispersive spectrometers, there is a trade-off between spectral bandwidth and spectral resolution, both determined by the pitch of the grating used. In addition, the spectral resolution is improved by closing the spectrometer slit.
8	When using the 'open pinhole' fiber, optimum spectral resolution is achieved by closing the slit blades of the spectrometer narrower than the image of the fiber core on the entrance slit, thereby rejecting parts of the fiber emission, and reducing the signal intensity. For some LPs or imaging conditions, an increase in acquisition time should be considered when high spectral resolution is needed.

93 Two representative parameter settings for different measurements are shown in Table 1 and 2 below. Parameter set 1 was used for a high-speed refractive index sensing experiment with polystyrene microbead LPs, where the settings were optimized for speed and spectral resolution. Parameter set 2 was used for a long-term cell tracking experiment with semiconductor nanodisk LPs, where 8 scans of identical settings were run back-to-back to track the cells for 68 h. Here, spatial resolution was given priority over scan speed. For both measurements, we limited the number of pixels read-out by the line-scan camera to the spectral bandwidth of interest, such that the amount of data generated was minimized. It is advisable to acquire and analyze a few test images of LPs in the same sample to confirm that the selected acquisition parameters lead to good quality images and spectra before proceeding.

Table 1 | Spatial parameters for typical hyperspectral scans

	Mag (NA)	FOV (mm)	voxel (µm)	pinhole (µm)	LP d/h (µm)	# buffers
1	10x (0.45)	1.6 × 1.6 × 0.8	5.2 × 5.2 × 40	105	15	380
2	25x (1.05)	0.48 × 0.48 × 0.04	1.3 × 1.3 × 1	10	1.8/0.2	480

Parameters: Objective magnification and NA (**Mag (NA)**); size of the FOV and of each voxel in x, y, and z (**FOV** and **voxel**); diameter of the optical fiber (**pinhole**); diameter and where applicable height of the LPs imaged (**LP d/h**); total number of camera buffers of one continuous scan (**# buffers**).

Table 2 | Temporal and spectral parameters of typical hyperspectral scans

	dt (µs)	frame (s)	stack (min)	scan (h)	# pixel λ	G (l/mm)	Δλ (nm)
1	34	3.02	0.96	0.32	680	1200	0.06
2	419	60.7	40.45	8.1	600	300	0.24

Parameters: Pixel dwell time (**dt**); time to image one x-y plane (**frame**), one z-stack (**stack**) and the entire hyperspectral scan (**scan**); number of pixels on the line-scan camera that were read out (**# pixel λ**); pitch of the grating used during the measurement (**G**); spectral resolution achieved in the resulting spectra (**Δλ**).

94 Start the acquisition. Long-term measurements can run without supervision, and remote access to the PC can be used to save data or restart the scan during the measurement.

▲ **CRITICAL** Long-term measurements with living cells likely require control of temperature and CO_2, for which we recommend using an on-stage incubator.

! **CAUTION** Prior to leaving during a long-term measurement, ensure that it is safe to operate the laser without supervision, and take precautions to prevent others from entering the lab.

General Data Processing ● TIMING 0.5 d

95 Open a python file or jupyter notebook, import the required modules (Supplementary Code 1, Cell 1). In addition to common scientific libraries, import utils.py (provided along with our code package), which contains elementary data processing functions.

96 To organize the file structure returned by the HyperspectralConfocal software into correct spatial, spectral, and temporal axes, a custom data structure called the acquisition class is used. It stores key acquisition parameters and contains data processing methods, which can directly access the acquisition parameters relevant for correct processing. Any data processing workflow starts by creating an instance of the acquisition class. Call the constructor of the acquisition class, using the name of the directory and the data set as inputs (Supplementary Code 1, Cell 2).
? TROUBLESHOOTING

97 Calibrate the acquisition by calling the autoCalibrate method, which takes the name of the log file as the first argument, and the scan field size of your objective at ±50 V (the number determined during Step 72, in µm) as the second argument (Supplementary Code 1, Cell 3).

98 You can also access and change all attributes of the acquisition directly, which also allows overwriting the automatic calibration and uploading data sets from different cameras (Supplementary Code 1, Cell 4).

99 Create hyperspectral images of individual x-y-planes with the construct2D method. For this, you need to specify the planes in z and t from which you want to extract the 2D image. The default version of this function creates an intensity image of the destination plane, which is displayed as one of two panels in a figure, and it returns the intensity counts as a 2D numpy array.

100 Optionally, the method can display and return an additional image containing the positions of the dominant lasing peaks (Supplementary Code 1, Cell 5). Additional keyword arguments allow adjusting thresholds and color scaling of the results (Supplementary Note 3).

101 To extract a single spectrum, determine the x-y position of the pixel of interest at a certain timestep and z-plane.

102 Call the getSingleSpectrum method, using x, y, z, and t as inputs. This method will retrieve the spectrum at the designated position from the original data set and return it as a numpy array, which can optionally be saved as a text file at a specified file path (Supplementary Code 1, Cell 6).

103 Multidimensional, pre-processed data sets can be displayed in the interactive python viewer napari[53]. Process the stack or time series, using the construct3D or 25onstruct methods for obtaining intensity images, or the constructSpec3D or constructSpecT methods for spectral color-coding (Supplementary Code, Cell 7).

104 To display intensity images, directly load them into the napari viewer, passing the correct spatial calibration, which is stored in the acquisition object, into the napari function call (Supplementary Code, Cell 8).

105 To display spectral data, apply the custom RGBA mapping to the processed images. This method encodes the spectral information as hue in three different color channels, with the brightness corresponding to the real intensity values.

106 Display the resulting ND-RGBA channels in napari, and apply the correct spatial scaling as described for the intensity images above (Supplementary Code, Cell 9).

107 To store the processed images, save screenshots of the viewer window by defining the path of the saved image.

108 To save a series of images, e.g., to create videos of time series or flyovers, create a loop that iterates over different timesteps and/or angles, saving an image at each iteration (Supplementary Code, Cell 10).

Box 5 | A: Analysis for Multi-mode Spectra ● TIMING 1-2 d

1 First, create a folder called 'fitted' in your working data directory, where all results of the fitting steps will be stored.

2 Batch-process the images in the data set to detect lasing peaks and store their spatial, spectral, and temporal position in pre-processed text files.

   i. For regular hyperspectral confocal data sets, call the fitSpectraToFiles method (Supplementary Code 2, Cell 1). The processed text files are organized into separate columns for each spectrum, where each columns holds information on the position and intensity of the lasing spectrum, followed by a list of the detected peaks, whose precise peak position is determined by fitting a gaussian to the experimental data.

   ii. Specify additional settings for the peak detection, which are explained in Supplementary Note 3.

   iii. Alternatively, one can batch-process ascii files containing a sequence of spectra, which would be beneficial to apply our multi-mode spectra routine to a data set acquired on a different camera (e.g., Andor Newton camera). To use the ascii function, ensure the ascii file contains the wavelength axis information in its first column, and the spectra in all following columns, which will be interpreted as spectra from a single position at consecutive time-step (Supplementary Code 2, Cell 2).

3 Open the asymptoticExpansion script in MATLAB. Change the name of the source directory and data set to match the acquisition to be processed.

4 Define the upper and lower bounds used for optimization of the three free parameters of the model (i.e., the microbead LP diameter, the radial mode number m, and the external refractive index).
   ▲ CRITICAL Setting the bounds incorrectly will lead to poor fitting results. Narrower bounds can increase the accuracy of the fit, but also increase the risk of excluding the correct values. Start with spectra from LPs embedded in a medium of homogenous, well-known refractive index to optimize the bounds for the bead diameter, before fitting spectra with a variable external refractive index.

5 Run the script to batch-process all files in the source directory containing the specified name. The script will optimize the two free parameters and add them to the end of each column in the result files. Additionally, the residual error of the mode positions for each fit is added to the columns.
   ? TROUBLESHOOTING

6 Generate result traces from fixed positions (RIU vs time) (Supplementary Code 2, Cells 3-4).

7 Fitted results from hyperspectral confocal scans can be displayed as images with custom color-coding representing various physical quantities. Call the cmapResultsFromFiles and specify which parameter is imported in the returned RGBA maps (fitted refractive index, fitted bead diameter, or the lasing peak position; Supplementary Figure 12 and Supplementary Code 2, Cell 5).

8 Display the ND-RGBA results in napari and export screenshots as described in Steps 106-108 (Supplementary Code 2, Cell 6-7).

9 More accurate results for the absolute refractive index can be achieved with the following calibration step, using spectra obtained from LPs embedded in a medium of homogenous, well-known refractive index such as DIW (e.g., the data measured at Steps 83-85). This calibration must be repeated whenever a new batch or type of LPs is used.

   i. Detect the lasing peaks following the same instructions as Box 5, Step 2. Open the asymptoticExpansionCalibration script in MATLAB and change the name of the data set and directory.

   ii. Specify the known refractive index of your calibration data set, e.g., 1.33 for DIW.

   iii. Leave the bounds of the diameter relatively open to account for divergence from the nominal size of the microbead lasers.

   iv. The script will return an internal refractive index and the spread of bead diameters. Update the internal refractive in the fitting script (Box 5, Step 4-5) and the bounds of the diameter to reflect the size spread measured during the calibration.

10 For LPs with any surface treatments or coatings, we advise to perform the calibration step prior to coating of the LP. An additional measurement of the coated LPs in a medium of well-known refractive index is recommended to quantify the effect of the surface coating on measurement of the external refractive index.

Box 6 | B: Analysis for Single-mode Spectra ● TIMING 2-3 d

1. Batch-process the data set into x-y-image files organized into a hypercube with z, λ, and t encoded as axis labels. To reduce the size of the resulting data set and speed up to subsequent steps, we have implemented a keyword argument that allows binning (Supplementary Code 3, Cell 1).
2. Add all processed files to a .zip folder by specifying source directory and filename identifier (Supplementary Code 3, Cell 2). You can now delete the batch-processed images from the directory.
   ▲ **CRITICAL** Ensure no additional files with the same filename identifier are in the working directory.
3. Feed the .zip folder into the ND tracking algorithm TrackPY[54] and run the batch-autodetection. The 'batch' method detects objects at each individual timestep by grouping pixels with similar positional and wavelength values into one object (Supplementary Code 3, Cell 3).
4. Run the linking algorithm to track the detected objects across multiple timesteps and export the results as Excel spreadsheet (Supplementary Code 3, Cell 4). The algorithm will return the tracked centroids of objects in the x-y-z-λ-t parameter space.
5. Create an instance of the trackingData class, which organizes the output from the tracking algorithm, using the name of the tracking data file as an input argument, and the acquisition object created during Box 6, Step 1 (Supplementary Code 3, Cell 5).
6. Display trajectories as images or extract traces of position or wavelength of individual tracked LPs (Supplementary Code 3, Cell 6).

Timing

Procedure I

Steps 1-10, Preparation of Polystyrene Microbead LPs: 2-3 h
Box 2, Steps 1-13, Preparation of bespoke Semiconductor LPs: 1-2 h
Steps 11-14, Adding LPs to Cells: 1 h
Steps 15-22, Fluorescence Microscopy Bioassay: 2-3 h
Steps 23-27, Fluorescence-Activated Cell Sorting: 0.5 d

Procedure II

Steps 1-6, PC Setup and Installation: 1 d
Steps 7-19, Construction of the Confocal Scanning: 1 d
Steps 20-33, Alignment of the Detection: 2-3 h
Steps 34-63, Camera Configuration and Alignment: 1 d
Steps 64-77, Calibration and Test Image Acquisition: 0.5 d
Steps 78-90, LP Reference Measurements: 2-3 d
Steps 91-94, Acquisition of Experimental Data: 2-3 h
Steps 95-108, General Data Processing: 0.5 d
Box 5, Steps 1-9, A: Analysis for Multi-mode Spectra: 1-2 d
Box 6, Steps 1-6, B: Analysis for Single-mode Spectra: 2-3 d

Troubleshooting

Procedure, Step	Problem	Possible Reason	Solution
I, 5	LPs do not form a clear pellet during centrifugation	LPs adhere to the walls of the microcentrifuge tube	After removing the supernatant, gently rinse the sidewalls of the microcentrifuge during resuspending of the LPs. Additional sonication steps can also be used to detach the LPs from the sidewalls. Alternatively, different solvents such as ethanol may be used during the centrifugation step to aid the formation of a well-defined pellet[56]; however, any remaining solvent must be removed completely prior to seeding the LPs with cells.
I, 5 (Box 2)	The wafer piece breaks during sonication.	The wafer was cleaved inappropriately or handled incorrectly, for example with a metal tweezer.	If shards or debris of toxic wafer are visible in the tube, dispose of the sample as small pieces of wafer cannot be filtered. Prepare a new sample, handling the wafer more diligently and using a plastic tweezer with flat edges where possible.
I, 8 (Box 2)	LPs are not detached.	The wafer piece was not positioned correctly during sonication, or the cell culture medium may not be suitable for detachment of semiconductor LPs.	Ensure that the wafer piece does not flip during sonication, and that the surface containing LPs is in close proximity to the tube wall (if this is challenging, cleave the wafer into slightly smaller pieces). One can alternatively use D-PBS solution to sonicate the LPs, following the same procedure. However, we do not recommend keeping the cell culture in D-PBS during the uptake period. Therefore, when detaching the cells in D-PBS, the LPs can be centrifuged at 12,000 G for 5 min. Remove the supernatant, resuspended LPs in cell medium, and sonicate the mixture for 5 min to avoid LP agglomeration.
I, 13	Density of LPs in final suspension is too low.	The preparation procedure was not efficient enough or the quantity used at the start was too low.	Centrifuge the LPs at 12,000 G for 5 min. A pellet of LPs should be visible by eye in the tube, or, if the number is low, by imaging the tube base with a 4× objective. Remove the supernatant, resuspended LPs in a smaller volume of cell medium, and sonicate the mixture for 5 min.
I, 14	Contamination of the cell culture.	Seeding of the LPs can be a source of contamination of the cell culture.	Equipment including tweezers, tubes, and filter holders can be autoclaved to ensure sterility. Equipment that cannot be autoclaved can be sterilized with IPA/EtOH or subjected to UV light in the cell culture hood. Tubes must be firmly shut and subsequently sealed with parafilm prior to sonication.
II, 9	Communication to DAQ cannot be established.	The name assigned to your DAQ differs from the name in NewGPScan.vi.	Assign a different name to your DAQ, or change the name in NewGPScan.vi, such that they are consistent.
II, 40	The blades of the spectrometer slit appear blurry or angled.	The CCD Camera is misaligned.	Re-align the z-position of the CCD camera (blades blurry) or its rotation (blades angled). The instruction manuals of most spectrometers recommend specific alignment strategies which should be followed.

|			
II, 58	The spectrum does not show any signal.	Camera communication is configured incorrectly.	First confirm that the camera is being triggered and that the measured spectrum is refreshing. Then ensure that the communication settings of the camera match those of the frame grabber. We include camera configuration files on our hardware repository; these can be loaded directly into the camera software to match our acquisition settings.
II, 70	The entire image is red.	The image is oversaturated.	Increase the conversion threshold in the camera software (up to 1300, if needed). If the image is still oversaturated, acquire another image with decreased light intensity.
II, 70	The entire image is blue.	The signal level is too low, or the camera is configured incorrectly.	First, increase the light intensity or decrease the conversion threshold. If this does not resolve the problem, repeat Step 36 to confirm the camera communication is set up correctly, and Steps 57-58 to check the camera alignment.
II, 70	The image is clipped on the edges.	The galvo scanner is misaligned.	At ± 50 V, some clipping on the edges is expected (see Supplementary Figure 8). Ensure the clipping is symmetric and does not persist at smaller scanning amplitudes than ca. ±45 V. Revisit Steps 15-18 for galvo alignment. If this does not resolve the clipping, the excitation path might be misaligned. To resolve this, center the galvos by observing light from the illumination LED on the alignment targets before and after the galvos. Then, realign the excitation beam to be centered in the conjugate image plane.
II, 70	The image is blurry.	The camera tube lens is at the wrong position.	Acquire a z-stack and compare the confocal and brightfield images at each slice. If there is a mismatch in terms of which slice shows the sharpest image, realign the camera tube lens (Steps 20-23).
II, 2 (Box 3)	The microbead lasers are not distributed evenly in the sample.	Microbead lasers are clumped together or have all sunk to the bottom of the stack.	For aggregates of microbead lasers, shake the bead stock more thoroughly before extracting the microbead lasers or sonicate it if necessary. If the microbead lasers sink to the bottom of the stack rather than staying evenly dispersed, ensure that the time between adding the LPs and putting the sample in the fridge is as short as possible. If necessary, use slightly higher concentrations of agarose in DIW.
II, 86	The intensity decreases throughout the sequence.	Photobleaching of the dye.	Decrease the excitation intensity or repetition rate. (The pulse power should however not be below the lasing threshold.) If this leads to poor signal-to-noise ratio, confirm that the light collection is well aligned and/or use a higher NA objective for more efficient light collection. If more signal is needed, increasing the pixel dwell time or excitation repetition rate is gentler on the microbead lasers than increasing the excitation energy. For FluoRed microbead lasers, in our experience a combination of scanning parameters can be found using a 10× (NA=0.45) objective, such that the intensity is stable with good signal-to-noise ratio (Supplementary Figure 13).
II, 86	A shadow artefact appears on the edge of the image.	The scan speed is too high, leading to non-linear movement of the galvos.	Increase the pixel dwell time or add more pixels per line to decrease the line rate. If higher speed is desired, the edge effect can be accepted and the images can be cropped; however, this makes the system more prone to imaging errors.

II, 90	The sectioning in z is much poorer than the expected PSF (e.g., Supplementary Figure 14).	The back aperture is underfilled, the pinhole size is not suitable, or the pinhole is not aligned correctly.	Confirm that the beam profile behind FC2 is homogenous and larger in size than the back aperture of the used objective. Using the fiber entrance as confocal pinhole can further improve z-resolution. For our combination of lenses, a 'closed pinhole', i.e., a pinhole size that is comparable to the size of the airy disk at the fiber entrance, is obtained with a 10 μm core fiber.
II, 96	The code returns a 'File not found' error.	The image was exported as single buffer, not as sequence.	The script expects entire ND-datasets exported as a sequence of buffers, which include an extension indicating the frame number at the end of the filename. Always export the final data set with the 'Save Seq' function, which also works if the data set consists of a single buffer. If this was not done, one can also manually change the filename to include the correct extension.
II, 5 (Box 5)	The results of the fit seem non-physical.	The fit might have converged to an incorrect solution.	Ensure the data set is calibrated appropriately (Box 5, Step 9). If possible, draw narrower bounds around all well-known parameters in the MATLAB script. Data from a more monodisperse set of microbead LPs is easier to fit correctly, as narrow size distributions allow narrow bounds on the size parameter. For best success with refractive index sensing, extract and analyze data from individual microbead LPs separately. For a given LP, determine the size, and then fix the size and fit all spectra allowing only the refractive index to vary[8]. The residual error from each fit, which is included with the result file in units of wavelength (m), should be smaller than the spectral resolution for successful convergence (i.e., 40 pm in our case).

Anticipated results

We described the integration and operation of intracellular LPs for cell tracking and intracellular sensing applications. Procedure I of our protocol, describing the integration of LPs into cells, has proven successful for the internalization of commercially available fluorescent microbead LPs by various types of cells, including primary macrophages, microglia, HEK 293, NIH 3T3[1], Hela, N7, SH-SY5Y[3], HL-1, and neonatal cardiomyocytes [8]. The cellular uptake of LPs can be enhanced drastically by including a liposome surface treatment step, but the level of improvement depends on the cell type[3]. More compact LPs, such as semiconductor nanodisk lasers, are readily integrated into primary macrophages, T cells, primary neurons, NIH 3T3[17], HL-1[57], and HEK 293 cells[10], as well as primary keratinocytes (Figure 8a). Procedure II of the protocol provides spectral imaging routines to obtain and analyze lasing signals from within living cells. Continuous acquisition of lasing spectra allows to use the peak emission wavelengths of LPs as unique identifiers to track cellular migration in 3D. Here, we demonstrate this by tracking primary keratinocytes labelled with semiconductor nanodisk LPs for 68 hours during their stratification into a 3D epidermis model[58] (Figure 8b,c).

Further, LPs can be used for real-time sensing of the local refractive index. In our previous work, we integrated polystyrene microbead LPs into cardiomyocytes (Figure 8d) and continuously monitored their lasing spectra to perform real-time sensing of cardiac contractility (Figure 8e)[8]. Our analysis script can extract the diameter of the LP and the external refractive index (Figure 8f) and is included with this protocol. Combined with the high-speed hyperspectral confocal imaging, extended 3D volumes containing LPs can be analyzed to generate volumetric maps of absolute refractive index (Figure 8g, Supplementary Video 1). In the measurement

presented here, polystyrene microbead LPs were embedded in an agarose matrix and continuously imaged for 20 minutes at an imaging rate of 58 s per complete z-stack (1.6 mm × 1.6 mm × 0.8 mm). This allowed us to monitor the diffusion of a high-refractive-index glucose solution through the sample by extracting the evolution of absolute refractive index from the spectra of individual LPs (Figure 8h).
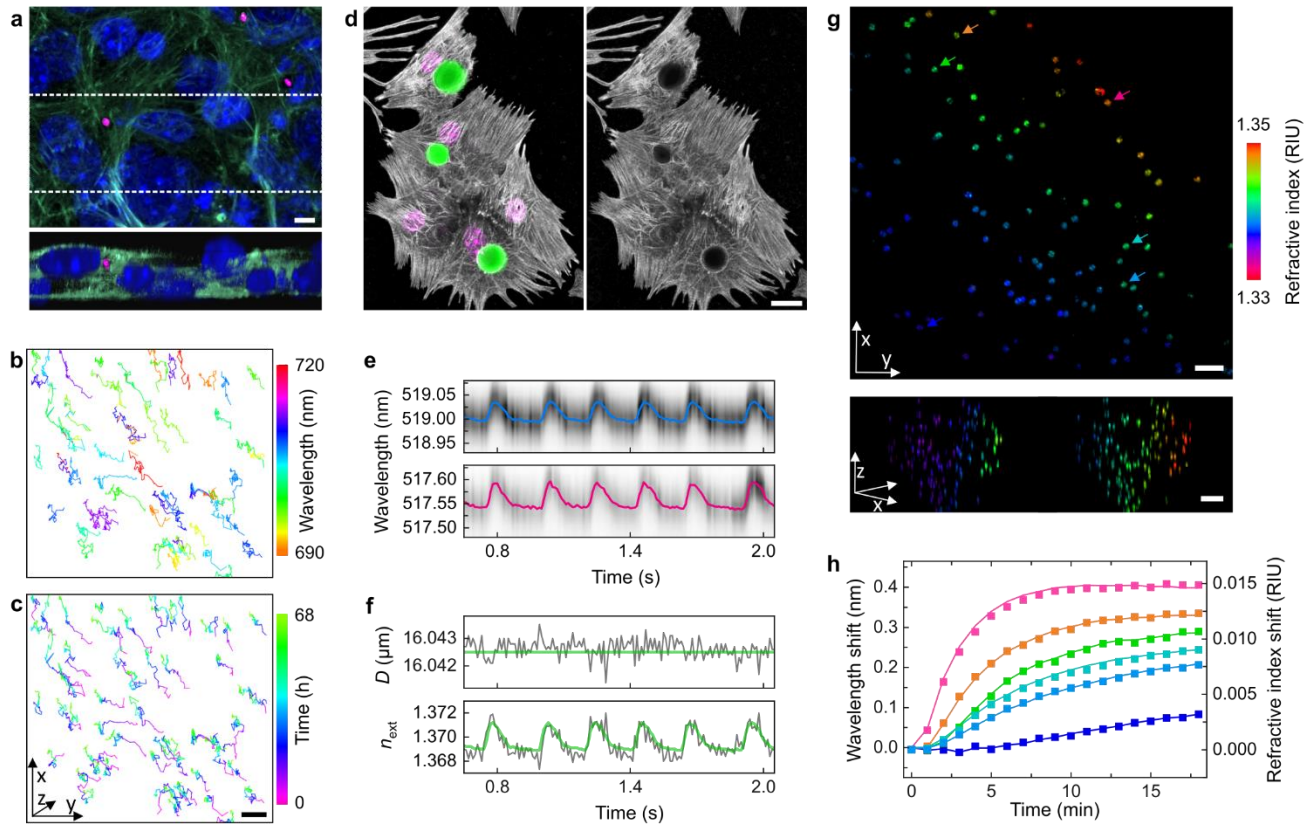
Figure 8 a, Integration of semiconductor nanodisk LPs (magenta) into a 3D cell culture model of primary keratinocytes, x-y (top) and x-z (bottom) maximum intensity projection (MIP) obtained with a commercial confocal microscope, showing cell nuclei (Hoechst, blue) and F-actin (phalloidin, green). Scale bar, 5 µm. The dashed lines indicate the section included in the x-z MIP. **b**, Tracked migration paths of individual keratinocytes, x-y MIP color-coded for LP emission wavelength and **c**, time. Scale bar, 50 µm. **d**, Confocal microscopy of polystyrene microbead LPs integrated into cardiomyocytes. MIP showing the LPs (green), sarcomeric protein cardiac troponin T (grey), and cell nuclei (magenta, left) and only the sarcomeric protein cardiac troponin T channel (right). Scale bar, 20 µm. **e**, Intracellular sensing of cardiac contractility by monitoring the lasing wavelength of multiple peak positions in multi-mode lasing spectra and **f**, subsequently extracting the external refractive index and diameter of the LP by either applying free fitting of the diameter (grey line) or the mean diameter (green line). **g**, Hyperspectral confocal images displaying results of a high-throughput refractive-index sensing measurement that follows the diffusion of glucose through an agarose matrix; x-y MIP (top, t = 8 min; scale bar, 100 µm) and x-z MIP (bottom, t = 3 min (left) and t = 16 min (right); scale bar, 200 µm). **h**, Changes in external refractive index for LPs located at the 3 locations indicated by arrows of corresponding color in g over the 20-minute scan.

Acknowledgements

Data availability

The research data supporting this publication can be accessed at [DOI to be assigned upon acceptance].

Code availability

A repository containing the SI code files can be found at https://github.com/GatherLab/sphyncs[55]. Custom hardware control software is available upon request.

References

1. Schubert, M. *et al.* Lasing within Live Cells Containing Intracellular Optical Microresonators for Barcode-Type Cell Tagging and Tracking. *Nano Lett* **15**, 5647–5652 (2015).

2. Humar, M. & Yun, S. H. Intracellular microlasers. *Nat Photonics* **9**, 572–576 (2015).

3. Schubert, M. *et al.* Lasing in Live Mitotic and Non-Phagocytic Cells by Efficient Delivery of Microresonators. *Sci Rep* **7**, 1–9 (2017).

4. Li, X. *et al.* In vivo tracking of individual stem cells labeled with nanowire lasers using multimodality imaging. *Biomed Opt Express* **13**, 4706 (2022).

5. Martino, N. *et al.* Wavelength-encoded laser particles for massively multiplexed cell tagging. *Nat Photonics* **13**, 720–727 (2019).

6. Foreman, M. R., Swaim, J. D. & Vollmer, F. Whispering gallery mode sensors. *Adv Opt Photonics* **7**, 168 (2015).

7. Su, J. Label-Free Biological and Chemical Sensing Using Whispering Gallery Mode Optical Resonators: Past, Present, and Future. *Sensors* **17**, 540 (2017).

8. Schubert, M. *et al.* Monitoring contractility in cardiac tissue with cellular resolution using biointegrated microlasers. *Nat Photonics* **14**, 452–458 (2020).

9. Kavčič, A. *et al.* Deep tissue localization and sensing using optical microcavity probes. *Nat Commun* **13**, 1269 (2022).

10. Titze, V. M., Caixeiro, S., Di Falco, A., Schubert, M. & Gather, M. C. Red-Shifted Excitation and Two-Photon Pumping of Biointegrated GaInP/AlGaInP Quantum Well Microlasers. *ACS Photonics* **9**, 952–960 (2022).

11. Gather, M. C. & Yun, S. H. Single-cell biological lasers. *Nat Photonics* **5**, 406–410 (2011).

12. Wei, Y. *et al.* Starch-Based Biological Microlasers. *ACS Nano* **11**, 597–602 (2017).

13. Humar, M. & Yun, S. H. Whispering-gallery-mode emission from biological luminescent protein microcavity assemblies. *Optica* **4**, 222 (2017).

14. Lee, S. S., Kim, J. Bin, Kim, Y. H. & Kim, S.-H. Wavelength-tunable and shape-reconfigurable photonic capsule resonators containing cholesteric liquid crystals. *Sci Adv* **4**, 8276–8298 (2018).

15. Hales, J. E., Matmon, G., Dalby, P. A., Ward, J. M. & Aeppli, G. Virus lasers for biological detection. *Nat Commun* **10**, (2019).

16. Xu, Z. *et al.* Random Lasing from Label-Free Living Cells for Rapid Cytometry of Apoptosis. *Nano Lett* **22**, 172–178 (2022).

17. Fikouras, A. H. *et al.* Non-obstructive intracellular nanolasers. *Nat Commun* **9**, 4817 (2018).

18. Lv, Z. *et al.* Intracellular near-Infrared Microlaser Probes Based on Organic Microsphere-SiO2 Core-Shell Structures for Cell Tagging and Tracking. *ACS Appl Mater Interfaces* **10**, 32981–32987 (2018).

19. Tang, S.-J. *et al.* Laser particles with omnidirectional emission for cell tracking. *Light Sci Appl* **10**, 23 (2021).

20. Tang, S. K. Y. *et al.* A multi-color fast-switching microfluidic droplet dye laser. *Lab Chip* **9**, 2767–2771 (2009).

21. Richter, D., Marinčič, M. & Humar, M. Optical-resonance-assisted generation of super monodisperse microdroplets and microbeads with nanometer precision. *Lab Chip* **20**, 734–740 (2020).

22. Humar, M., Muševič, I., Sullivan, K. G. & Hall, D. G. 3D microlasers from self-assembled cholesteric liquid-crystal microdroplets. *Opt Express* **18**, 26995–27003 (2010).

23. Chen, Y. C. *et al.* Monitoring Neuron Activities and Interactions with Laser Emissions. *ACS Photonics* **7**, 2182–2189 (2020).

24. Wu, X. *et al.* Nanowire lasers as intracellular probes. *Nanoscale* **10**, 9729–9735 (2018).

25. Hua, B., Motohisa, J., Kobayashi, Y., Hara, S. & Fukui, T. Single GaAs/GaAsP Coaxial Core–Shell Nanowire Lasers. *Nano Lett* **9**, 112–116 (2009).

26. Feng, C. *et al.* Organic-Nanowire-SiO2 Core-Shell Microlasers with Highly Polarized and Narrow Emissions for Biological Imaging. *ACS Appl Mater Interfaces* **9**, 7385–7391 (2017).

27. Fernandez-Bravo, A. *et al.* Continuous-wave upconverting nanoparticle microlasers. *Nat Nanotechnol* **13**, 572–577 (2018).

28. Wang, S. *et al.* High-Yield Plasmonic Nanolasers with Superior Stability for Sensing in Aqueous Solution. *ACS Photonics* **4**, 1355–1360 (2017).

29. Caixeiro, S., Gaio, M., Marelli, B., Omenetto, F. G. & Sapienza, R. Silk-Based Biocompatible Random Lasing. *Adv Opt Mater* **4**, 998–1003 (2016).

30. Mysliwiec, J., Cyprych, K., Sznitko, L. & Miniewicz, A. Biomaterials in light amplification. *Journal of Optics* **19**, 033003 (2017).

31.   Cho, S., Yang, Y., Soljačić, M. & Yun, S. H. Submicrometer perovskite plasmonic lasers at room temperature. *Sci Adv* **7**, 3362–3387 (2021).

32.   Yu, D. *et al.* Whispering-gallery-mode sensors for biological and physical sensing. *Nature Reviews Methods Primers* **1**, 83 (2021).

33.   Liu, P. Y. *et al.* Cell refractive index for cell biology and disease diagnosis: past, present and future. *Lab Chip* **16**, 634–644 (2016).

34.   Chan, K. K. *et al.* Monitoring Amyloidogenesis with a 3D Deep-Learning-Guided Biolaser Imaging Array. *Nano Lett* **22**, 8949–8956 (2022).

35.   Chen, Q. *et al.* Highly sensitive fluorescent protein FRET detection using optofluidic lasers. *Lab Chip* **13**, 2679–2681 (2013).

36.   Oki, O. *et al.* FRET-mediated near infrared whispering gallery modes: Studies on the relevance of intracavity energy transfer with Q-factors. *Mater Chem Front* **2**, 270–274 (2018).

37.   Yuan, Z., Wang, Z., Guan, P., Wu, X. & Chen, Y. C. Lasing-Encoded Microsensor Driven by Interfacial Cavity Resonance Energy Transfer. *Adv Opt Mater* **8**, 1–9 (2020).

38.   Wang, Y. *et al.* Demonstration of intracellular real-time molecular quantification via FRET-enhanced optical microcavity. *Nat Commun* **13**, (2022).

39.   Li, X. *et al.* Optical coherence tomography and fluorescence microscopy dual-modality imaging for in vivo single-cell tracking with nanowire lasers. *Biomed Opt Express* **11**, 3659 (2020).

40.   Champion, J. A. & Mitragotri, S. Role of target geometry in phagocytosis. *Proceedings of the National Academy of Sciences* **103**, 4930–4934 (2006).

41.   Gratton, S. E. A. *et al.* The effect of particle design on cellular internalization pathways. *Proceedings of the National Academy of Sciences* **105**, 11613–11618 (2008).

42.   Stewart, M. P., Langer, R. & Jensen, K. F. Intracellular Delivery by Membrane Disruption: Mechanisms, Strategies, and Concepts. *Chem Rev* **118**, 7409–7531 (2018).

43.   Wu, Y. C. *et al.* Massively parallel delivery of large cargo into mammalian cells with light pulses. *Nat Methods* **12**, 439–444 (2015).

44.   Cho, S., Humar, M., Martino, N. & Yun, S. H. Laser Particle Stimulated Emission Microscopy. *Phys Rev Lett* **117**, (2016).

45.   Humar, M., Upadhya, A. & Yun, S. H. Spectral reading of optical resonance-encoded cells in microfluidics. *Lab Chip* **17**, 2777–2784 (2017).

46.   Dannenberg, P. H. *et al.* Laser particle activated cell sorting in microfluidics. *Lab Chip* **22**, 2343–2351 (2022).

47.   Bednarkiewicz, A., Chan, E. M., Kotulska, A., Marciniak, L. & Prorok, K. Photon avalanche in lanthanide doped nanoparticles for biomedical applications: super-resolution imaging. *Nanoscale Horiz* **4**, 881–889 (2019).

48.   Hill, M. T. & Gather, M. C. Advances in small lasers. *Nat Photonics* **8**, 908–918 (2014).

49.   Dannenberg, P. H. *et al.* Droplet microfluidic generation of a million optical microparticle barcodes. *Opt Express* **29**, 38109 (2021).

50. Liapis, A. C. *et al.* Conformal Coating of Freestanding Particles by Vapor-Phase Infiltration. *Adv Mater Interfaces* **7**, (2020).

51. Schindelin, J. *et al.* Fiji: an open-source platform for biological-image analysis. *Nat Methods* **9**, 676–682 (2012).

52. Ferrand, P. GPScan.VI: A general-purpose LabVIEW program for scanning imaging or any application requiring synchronous analog voltage generation and data acquisition. *Comput Phys Commun* **192**, 342–347 (2015).

53. Sofroniew, N. *et al.* napari: a multi-dimensional image viewer for python. (2022) doi:10.5281/zenodo.3555620.

54. Daniel B Allan, Thomas Caswell, Nathan C Keim, Casper M van der Wel & Ruben W Verweij. soft-matter/trackpy: Trackpy v0.5.0. (2021) doi:10.5281/zenodo.3492186.

55. Vera M Titze, Soraya Caixeiro, Marcel Schubert & Malte C Gather. GatherLab/sphyncs. (2023) doi:10.5281/zenodo.8121099.

56. Dannenberg, P. H. *et al.* Facile layer-by-layer fabrication of semiconductor microdisk laser particles. *APL Photonics* **8**, 021301 (2023).

57. Caixeiro, S. *et al.* Micro and nano lasers from III-V semiconductors for intracellular sensing. in *Enhanced Spectroscopies and Nanoimaging 2020* vol. 11468 1146811 (2020).

58. Rübsam, M. *et al.* E-cadherin integrates mechanotransduction and EGFR signaling to control junctional tissue polarization and tight junction positioning. *Nat Commun* **8**, (2017).

Primary References

Schubert, M. *et al.* Lasing in Live Mitotic and Non-Phagocytic Cells by Efficient Delivery of Microresonators. *Sci Rep* **7**, 1–9 (2017).

Schubert, M. *et al.* Monitoring contractility in cardiac tissue with cellular resolution using biointegrated microlasers. *Nat Photonics* **14**, 452–458 (2020).

Titze, V. M., Caixeiro, S., Di Falco, A., Schubert, M. & Gather, M. C. Red-Shifted Excitation and Two-Photon Pumping of Biointegrated GaInP/AlGaInP Quantum Well Microlasers. *ACS Photonics* **9**, 952–960 (2022).